A *MSTN*^{Del273C} mutation with *FGF5* knockout sheep by CRISPR/Cas9 promotes skeletal muscle myofiber hyperplasia

Ming-Ming Chen[1, †], Yue Zhao[1, †], Xue-Ling Xu[1], Xiao-Sheng Zhang[2], Jin-Long Zhang[2], Su-Jun Wu[1], Zhi-Mei Liu[1], Yi-Ming Yuan[1], Xiao-Fei Guo[2], Shi-Yu Qi[1], Guang Yi[1], Shu-Qi Wang[1], Huang-Xiang Li[1], Ao-Wu Wu[1], Guo-Shi Liu[1], Kun Yu[1], Shoulong Deng[3], Hong-Bing Han[1], Feng-Hua Lv[1, *], Yan Li[4, *], Zheng-Xing Lian[1, *]

[1] Beijing Key Laboratory for Animal Genetic Improvement, National Engineering Laboratory for Animal Breeding, Key Laboratory of Animal Genetics and Breeding of the Ministry of Agriculture, College of Animal Science and Technology, China Agricultural University, Beijing 100193, China

[2] Institute of Animal Husbandry and Veterinary Medicine, Tianjin Academy of Agricultural Sciences, Tianjin 300381, China

[3] NHC Key Laboratory of Human Disease Comparative Medicine, Institute of Laboratory Animal Sciences, Chinese Academy of Medical Sciences and Comparative Medicine Center, Peking Union Medical College, Beijing, China

[4] Laboratory Animal Center of the Academy of Military Medical Sciences, Beijing 100071, China

† These authors contributed equally to this work.

* Correspondence: lianzhx@cau.edu.cn (Zheng-Xing Lian), scauly@cau.edu.cn (Yan Li); lvfenghua@cau.edu.cn (Feng-Hua Lv)

Abstract

Mutations in the well-known Myostatin (*MSTN*) produce a "double-muscle" phenotype, which makes it commercially invaluable for improving livestock meat production and providing high-quality protein for humans. However, mutations at different loci of the *MSTN* often produce a variety of different phenotypes. In the current study, we increased the delivery ratio of Cas9 mRNA to sgRNA from the traditional 1:2 to 1:10, which improves the efficiency of the homozygous mutation of biallelic gene. Here, a $MSTN^{Del273C}$ mutation with *FGF5* knockout sheep, in which the *MSTN* and *FGF5* dual-gene biallelic homozygous mutations were produced via the deletion of 3-base pairs of AGC in the third exon of *MSTN*, resulting in cysteine-depleted at amino acid position 273, and the *FGF5* double allele mutation led to inactivation of *FGF5* gene. The $MSTN^{Del273C}$ mutation with *FGF5* knockout sheep highlights a dominant "double-muscle" phenotype, which can be stably inherited. Both F0 and F1 generation mutants highlight the excellent trait of high-yield meat with a smaller cross-sectional area and higher number of muscle fibers per unit area. Mechanistically, the $MSTN^{Del273C}$ mutation with *FGF5* knockout mediated the activation of *FOSL1* via the MEK-ERK-FOSL1 axis. The activated *FOSL1* promotes skeletal muscle satellite cell proliferation and inhibits myogenic differentiation by inhibiting the expression of MyoD1, and resulting in smaller myotubes. In addition, activated ERK1/2 may inhibit the secondary fusion of myotubes by Ca^{2+}-dependent CaMKII activation pathway, leading to myoblasts fusion to form smaller myotubes.

Keywords: *MSTN*; *FGF5*; dual-gene biallelic mutation; *FOSL1*; myogenesis

1 Introduction

Myostatin (*MSTN*) has been well-known as a negative regulator of muscle growth and development. Its mutation produces a “double-muscle” phenotype, which shows its inestimable commercial value in improving meat production of livestock and poultry, and providing high-quality protein for humans (Fan *et al.*, 2022; Chen *et al.*, 2021b). Due to its role in promoting muscle atrophy and cachexia, *MSTN* has been recognized as a promising therapeutic target to offset the loss of muscle mass (Lee, 2021; Baig *et al.*, 2022; Wijaya *et al.*, 2022).

MSTN is highly conserved in mammals, and mutations in the *MSTN* gene, either artificially or naturally, will result in increased skeletal muscle weight and produce a “double-muscle” phenotype, which has been reported in many species, including cattle, sheep, and pigs, rabbits, and humans (Grisolia *et al.*, 2009; Dilger *et al.*, 2010; Kambadur *et al.*, 1997). However, mutations at different loci of the *MSTN* often produce variety of different phenotypes, and its molecular mechanism of skeletal muscle growth and development remains controversial (Hanset and Michaux, 1985; Grobet *et al.*, 1997; Wegner *et al.*, 2000; Kambadur *et al.*, 1997; Marchitelli *et al.*, 2003). More than 77 natural mutation sites of *MSTN* have been reported in various sheep breeds, most of these mutations were found to be located in the non-coding regions, and did not affect *MSTN* activity (Kijas *et al.*, 2007; Sjakste *et al.*, 2011; Han *et al.*, 2013; Dehnavi *et al.*, 2012). In addition to introns, it is still possible that mutations in regulatory regions and exons may not affect the sheep phenotypes (Pothuraju *et al.*, 2015; Kijas *et al.*, 2007; Boman and Vage, 2009; Boman *et al.*, 2009).

Fibroblast growth factor 5 (*FGF5*) belongs to the fibroblast growth factor (FGF) family and is a secretory signaling protein. *FGF5* played an inhibitory effect on mouse hair growth (Hebert *et al.*, 1994), and its natural mutation can lead to a significant increase in hair growth in angora mice (Sundberg *et al.*, 1997). Subsequent studies have also successively confirmed the inhibitory effect of *FGF5* on mammalian hair growth and is recognized to be a negative regulator of hair growth (Kehler *et al.*, 2007; Dierks *et al.*, 2013; Yoshizawa *et al.*, 2015; Legrand *et al.*, 2014; Higgins *et al.*, 2014).

In this study, to increase both meat and wool production, we first produced the *MSTN* and *FGF5* dual-gene biallelic homozygous mutations sheep by the increased delivery ratio of Cas9 mRNA to sgRNA targeting *MSTN* and *FGF5*. The *MSTN*^{Del273C} mutation with *FGF5* knockout sheep highlights a dominant "double-muscle" phenotype by decreasing the muscle fiber cross-sectional area and increasing the number of muscle fibers per unit area. Then, we used the *MSTN* and *FGF5* dual-gene biallelic homozygous mutations sheep to unravel the molecular mechanism of the "double-muscle" phenotype and myofiber hyperplasia.

2 Materials and Methods

2.1 Production of Cas9 mRNA and sgRNA

The Cas9 and U6-sgRNA co-expression vector backbones pX330 were purchased from Addgene (plasmid ID: 42230 and 48138). Sheep MSTN and FGF5 sgRNAs were designed using CRISPR Design Tool (http://tools.genome-engineering.org). The MSTN sgRNA (GACATCTTTGTAGGAGTACAGCAA) and FGF5 sgRNA (AGGTTCCCCTTTCCGCACCT) were used in this study. Two complementary guide sequence oligos were synthesized, annealed, and cloned into the pX330 backbone vector to form the functional co-expression plasmids. T7 promoter was linked to the 5' ends of the Cas9 coding region and MSTN/FGF5 sgRNA template by PCR amplification from the pX330-MSTN/FGF5 plasmid constructed as described above. Then, these PCR products, as transcription templates, were purified using E.Z.N.A. Cycle Pure Kit (Omega Bio-Tek). MSTN sgRNA and FGF5 sgRNA were prepared by in vitro transcription (IVT) using the MEGAshortscript T7 Kit (Life Technologies). Cas9 mRNA was transcribed with the m7G(5')ppp(5') G cap on its 5' terminal and poly (A) tail on its 3' terminal using the mMESSAGE mMACHINE T7 Ultra Kit (Life Technologies). Both the Cas9 mRNA and the sgRNAs were purified using the MEGAclear Kit (Life Technologies) and eluted in RNase-free water.

2.2 Microinjection and embryo transfer

The procedure for the efficient production of pronuclear embryos has been described previously (Li *et al.*, 2016). Briefly, Cas9 mRNA (1000 ng/μL) and

sgRNAs (200 ng/μL) were mixed and injected into the transferable embryos in which the zona pellucida was clear, cytoplasm was uniform, and pronucleus was visible using a FemtoJet microinjector (Eppendorf). Following microinjection, three to five embryos were transplanted into the oviduct of each recipient within 1 h after starting the laparotomy operation. Pregnancy was confirmed by transabdominal ultrasound scanning on the 60th day after embryo transfer.

2.3 Tissue sample collection and preparation

Gluteus medius and longissimus dorsi were harvested from WT and *MSTN*^{Del273C} mutation with *FGF5* knockout (MF$^{-/-}$) sheep, and three WT sheep and four MF$^{-/-}$ F1 generation sheep (half-sib) were used for feeding and slaughter. All sheep were female and are slaughtered at 12-month-old. All samples were immediately frozen in liquid nitrogen and then stored at −80°C until analysis. All sheep are raised by the national feeding standard NT/T815-2004. All procedures performed for this study were consistent with the National Research Council Guide for the Care and Use of Laboratory Animals. All experimental animal protocols in this study were approved and performed following the requirements of the Animal Care and Use Committee at China Agricultural University (AW02012202-1-3). All surgeries were performed under sodium pentobarbital anesthesia, and all efforts were made to minimize any suffering experienced by the animals used in this study.

2.4 H&E staining and morphological analysis of muscle fibers

Fresh muscle tissue samples were fixed, dehydrated, embedded and frozen sectioned, respectively. Next, they were sequentially stained with hematoxylin and eosin, then dehydrated with gradient ethanol and transparentized with xylene, and finally sealed with neutral resin to make tissue sections. The images from at least five random fields were captured with an inverted microscope. The Image J software was used to segment, count and calculate the area of each muscle fiber cell. The number of fiber cell in a fixed area size was calculated to estimate the number of fiber cell per unit area.

2.5 Cell isolation, culture, and transfection

Sheep skeletal muscle satellite cells were isolated and cultured as previously described (Chen *et al.*, 2021a). In brief, the muscle tissues of the hind limbs from 3-month-old sheep fetuses were cut into small pieces, digested sequentially with 0.2% collagenase type II (Gibco, Grand Island, NY) and 0.25% trypsin (Gbico, Grand Island, NY). The cell suspension was successively filtered through 100, 200 and 400 mesh cell sieves. After this, the cells were resuspended in growth medium (GM) containing DMEM/F12 (Gbico, Grand Island, NY) with 20% fetal bovine serum (FBS, Gibco) and 1% penicillin-streptomycin liquid (Gbico, Grand Island, NY), and cultured for 2-3 times with differential adhesion. To induce differentiation, the cells were cultured to 70% confluence in GM, and followed by an exchange to differentiation medium (DM) containing DMEM high glucose (Gbico, Grand Island, NY) with 2% horse serum (HS, Gibco) and 1% penicillin-streptomycin. To produce viral solution for over-expression of the target gene, it was subcloned into the XbaI and BamHI sites of the lentiviral vector by seamless cloning, and the primer sequences of gene cloning were listed in Table S1. HEK 293T cells were co-transfected with the envelope plasmid pMD2.G, the packaging plasmid psPAX2 and the target plasmid at a mass ratio of 1:2:4 to produce the virus. The siRNA were synthesized by Guangzhou RiboBio Co., Ltd, and the sequences were listed in Table S2. Then, the cells were infected with packaged lentivirus or transfected with siRNA using Lipofectamine 3000 (Invitrogen, USA) when they were cultured to 60%-70% confluence.

2.6 Total RNA isolation and real-time quantitative PCR (RT- qPCR)

The total RNA of tissues and cells was isolated using TRIzol reagent (Sangon Biotech, Shanghai, China) following the manufacturer’s protocol. In short, after tissues or cells were lysed, chloroform was added to separate the organic and inorganic phases, followed by precipitation with isopropanol and ethanol in turn, and finally, the RNA was dissolved in DEPC water. Then, the first strand cDNA was prepared using PrimeScript II 1st Strand cDNA Synthesis Kit (Takara, Beijing, China).

qPCR was performed using 2× SYBR Green qPCR Mix (Low ROX) (Aidlab Biotechnologies, Beijing, Chian) in a Stratagene Mx3000P (Agilent Technologies, SUA). With GAPDH mRNA as endogenous control, the relative expression level of genes was calculated by the $2^{-\Delta\Delta Ct}$ method. All primers used were listed in Table S3.

2.7 Western blot

Tissue or cell samples were lysed in RIPA buffer (Solarbio, Beijing, China) supplemented with protease and phosphatase inhibitor cocktail (Beyotime, Beijing, China) for total protein extraction. Then, equal amounts of tissue or cell lysate were resolved by 10% SDS-PAGE and transferred onto PVDF membranes (Millipore, USA). The membranes were blocked with 5% BSA for 1h, incubated with primary antibody at 4℃ overnight, then incubated with secondary antibody for 1h before detection. The fold change of protein was normalized to GAPDH for quantitative analysis by ImageJ software. The antibodies information was listed in Table S4.

2.8 5-Ethynyl-2′-deoxyuridine (EdU) assay

At 24 h after transfection, sheep skeletal muscle satellite cells were incubated at 37℃ for 2 h in 96-well plates with 50 μM EdU (RiboBio, Guangzhou, China). Then, fixed the cells in 4% paraformaldehyde for 30 min and neutralized using 2 mg/mL glycine solution. The Apollo® staining solution which contains EdU was added and incubated at room temperature for 30 min in the dark to label the DNA in the synthesis stage, the nuclear was then counterstained with DAPI. The number of EdU positive cells was counted from the images of five random fields obtained with an inverted fluorescence microscope at a magnification of 100×. EdU labeling index was expressed as the number of EdU-positive cell nuclei/total cell nuclei.

2.9 Cell counting kit-8 (CCK-8) and cell cycle detection

Skeletal muscle satellite cells were seeded in 96-well plates and cultured for appropriate time according to different experimental treatments. Then, 10 μL CCK-8 solution was added to each well and incubated at 37°C in a 5% CO_2 incubator for 2 h, and then the absorbance at 450 nm was measured with a microplate reader. The

cultured skeletal muscle satellite cells were digested with trypsin, centrifuged at 1000 g for 5 min to collect the cell pellet, washed once with ice-cold PBS, and then 1 mL of ice-cold 70% ethanol was added to fix the cells overnight at 4°C. The next day, the cells were washed with ice-cold PBS again, and the cells were incubated with 0.5 mL PI staining solution at 37°C for 30 min and collected by flow cytometry at low speed.

2.10 Immunofluorescence staining

Sheep skeletal muscle cells were fixed in 4% paraformaldehyde for 30 min, permeabilized in 0.1% Triton X-100 for 20 min and blocked with 5% normal goat serum for 30 min at room temperature, and then incubated with primary antibody at 4℃ overnight. Next, the fluorescent secondary antibody was added and incubated at 37℃ for 1 h in the dark, and the nuclear was then counterstained with DAPI. The immunofluorescence images from five random fields were captured with an inverted fluorescence microscope.

2.11 Chromatin Immunoprecipitation (ChIP)

The cells were fixed with 1% formaldehyde, then the cells were collected with a cell scraper and resuspended in cell lysis buffer (10 mM HEPES, 0.5% NP-40, 1.5 mM MgCl2, 10 mM KCl, pH 7.9) containing protease inhibitor cocktail (Beyotime, Beijing, China) and incubated on ice to release the cytoplasm. Next, cell pellets were collected and resuspended in nuclear lysis buffer (50 mM Tris, 10 mM EDTA, 0.3% SDS, pH 8.0) containing protease inhibitor cocktail. After the DNA was fragmented by ultrasonication, the supernatant was collected. The samples were diluted ChIP dilution buffer (0.01% SDS, 1.1% Triton X- 100, 1.2 mM EDTA, 16.7 mM Tris-HCl pH 8.0, 167 mM NaCl), then 5 μg primary antibody was added and incubated overnight at 4°C with rotation. The next day, protein A/G magnetic beads were added to each sample and incubated at 4°C with rotation for 2h. Then, the magnetic beads were respectively washed once with low-salt wash buffer (0.1% SDS, 1% Triton X-100, 2 mM EDTA, 20 mM Tris-HCl pH 8.0, 150 mM NaCl), high-salt wash buffer (0.1% SDS, 1% Triton X-100, 2 mM EDTA, 500mM NaCl, 20 mM Tris-HCl pH 8.0), LiCl wash buffer (0.25 M LiCl, 1% NP-40, 1% sodium deoxycholate, 1 mM EDTA,

10 mM Tris-HCl pH 8.0), and TE buffer (10 mM Tris-HCl pH 8.0, 1 mM EDTA) at 4°C. Next, ChIP elution buffer (1% SDS, 100 mM $NaHCO_3$) containing proteinase K was added to each sample, then incubated at 62°C overnight, and the DNA was finally purified by a purification column.

2.12 RNA-seq

The rRNA was removed from each total RNA sample of the gluteus medius to construct a strand-specific transcriptome sequencing library, and the Illumina Novaseq 6000 sequencing platform was used to perform high-throughput sequencing with a paired-end read length of 150 bp. Raw data were transformed into clean reads by removing reads containing adapter, ploy-N and low-quality reads from raw data. At the same time, Q20, Q30, GC-content, and sequence duplication levels of the clean data were calculated. The genome index was constructed using Hisat2 software and the clean reads were mapped to the sheep reference genome (*Oar Rambouillet v1.0*), the featureCounts software was used for expression quantification, and DESeq2 software was used for differential expression analysis based on *P*-value < 0.05 and | log2 Fold Change | > 1.

3 Results

3.1 Elevated molar ratio of Cas9/sgRNA can efficiently generate biallelic homozygous mutant sheep

The sgRNAs for targeting were designed in the third exon of the MSTN and FGF5 genes, respectively (Figure 1A, B). Both MSTN and FGF5 PCR products could be cleaved by T7E1 and the fragment sizes were also as expected, and grayscale analysis showed that the editing efficiency was 14.6% and 11.4%, respectively (Figure 1C), which indicates that the designed sgRNAs can achieve more efficient gene targeting. The microinjection was performed according to the molar ratio of Cas9 mRNA:sgRNAs (1:2, 1:10, and 1:15), respectively. The number of embryos injected, recipients of nuclear transfer, pregnancy, and alive lambs per group were listed in Table S5. The subsequent gene mutation detection showed that a total of 3 lambs were mutated in the MSTN and FGF5 genes at a Cas9 mRNA:sgRNAs injection molar ratio of 1:2, with a gene editing mutation rate of 14.3% (4/28).

However, all 3 lambs were chimeric, that is, there were both mutant and wild-type after editing, and the biallelic mutation rate was 0% (Table S5 , Figure 1D). Increasing the injection molar ratio of Cas9 mRNA:sgRNAs to 1:10 resulted in mutations in MSTN and FGF5 genes of two lambs with a gene editing mutation rate of 18.2 % (4/22), which contributed to a significant (P<0.05) increase in the biallelic mutation rate (Table S5, Figure 1D). While the injection molar ratio of Cas9 mRNA: sgRNAs was continuously increased to 1:15, one lamb had a mutation, which was a biallelic mutation of *MSTN* gene, and the gene editing mutation rate was 7.14% (1/14) (Table S5, Figure 1D). These results indicate that increasing the delivery molar ratio of Cas9 mRNA to sgRNA from 1:2 to 1:10 can greatly improve the efficiency of biallelic mutation in sheep.

3.2 The *MSTN*^{Del273C} mutation with *FGF5* knockout sheep highlights a dominant "double-muscle" phenotype and muscle fiber hyperplasia

Among gene-edited sheep, a sheep with biallelic deletion of *MSTN* and biallelic mutation of *FGF5* aroused our great interest. Specifically, gene editing caused a deletion of 3-base pairs of AGC in the third exon of *MSTN* (Figure 1E, F), resulting in the deletion of cysteine at amino acid position 273 (*MSTN*^{Del273C}) (Figure 1 E, F), which is highlighted by the "double-muscle" phenotype (Figure 2A, 2B). At the same time, a biallelic mutation in *FGF5* caused the knockout of *FGF5* gene and increased the density and length of hairs (Zhang *et al.*, 2020). Compared to WT sheep, the fiber cell number per unit area of gluteus medius and longissimus dorsi in MF$^{-/-}$ sheep was significantly (P<0.01) increased (Figure 2C, D), and the cross-sectional area were smaller (Figure 2C, E-F). Similarly, the cross-sectional area of gluteus medius muscle fibers in the offspring generation MF$^{+/-}$ sheep was also smaller (Figure 2G-H), and the number of muscle fiber cells per unit area was significantly increased (P<0.0001) (Figure 2G, I); the percentage of smaller muscle fiber area in MF$^{+/-}$ sheep was significantly increased (P<0.05) (Figure 2G, J), these results was consistent with that in MF$^{-/-}$ sheep. Interestingly, the FGF5 knockout alone had no significant (P>0.05) effect on muscle fiber size (Figure S1A-D). Although the mRNA expression levels of *MSTN* and *FGF5* were significantly (P<0.05) reduced in MF$^{+/-}$ sheep during early embryonic development (3-month-old) (Figure S2A), there was no significant

differences in *MSTN* mRNA and protein expression levels at 12-month-old after birth (Figure S2B-D). In addition, there was no significant differenc in the proportion of centrally nucleated myofibres (P>0.05) (Figure S2E), nor were there aberrant expression of some genes related to muscular dystrophy and muscle atrophy (Figure S2F). These results indicate that *MSTN*^{Del273C} mutation with *FGF5* knockout produces muscle fiber hyperplasia instead of muscular dystrophy or muscle atrophy.

Further, although the muscle weight of different parts in WT and MF$^{+/-}$ sheep has no significant difference (Table S6), the proportion of hind leg meat was significantly (P<0.05) increased by 21.2% (Table S7), and the proportion of gluteus medius in the carcass of MF$^{+/-}$ sheep was significantly (P<0.01) increased by 26.3% compared to WT sheep (Figure 2K). In addition, there were no significant (P>0.05) differences in pH, color, drip loss, cooking loss, shearing force, and amino acid content of the longissimus dorsi between WT and MF$^{+/-}$ sheep (Table S8-10). All these results demonstrated that the *MSTN*^{Del273C} mutation with *FGF5* knockout sheep had well-developed hip muscles with smaller muscle fibers, which do not affect meat quality, and this phenotype may be dominated by *MSTN* gene.

3.3 The *MSTN*^{Del273C} mutation with *FGF5* knockout promotes skeletal muscle satellite cells proliferation and inhibits myogenic differentiation

The proliferation and differentiation of skeletal muscle satellite cells is a key step in muscle formation and development. The CCK-8 and EdU cell proliferation experiments showed that the proliferative rate of MF$^{+/-}$ cells were highly significantly (P<0.01) elevated (Figure 3A) with a significant (P<0.05) increase in the rate of EdU-positive cells (Figure 3B, C) compared to WT cells. In addition, cell cycle detection showed a significant (P<0.01) reduce in the proportion of G1 phase and a significant increase (P<0.05) in the proportion of S phase in MF$^{+/-}$ cells (Figure 3D, E). Meanwhile, the mRNA expression levels of the cell cycle marker genes CyclinB1, CDK4, Cyclin A1, Cyclin E1, and CDK2 were significantly increased (P<0.05) (Figure 3F). These results suggest that the *MSTN*^{Del273C} mutation with *FGF5* knockout may promote cell proliferation by accelerating the cell cycle from G0/G1 phase to S phase.

The mRNA level of MyHC and the protein levels of MyoD1, MyoG, and MyHC (Figure 3G-I) were dramatically decreased (P<0.05) after induced differentiation 2 days in $MF^{+/-}$ cells, suggesting that the $MSTN^{Del273C}$ mutation with *FGF5* inhibit myogenic differentiation. Meanwhile, the immunofluorescence staining of MyoG and MyHC in myotubes showed that myotube fusion index (Figure 3J, K), number of myotubes (Figure 3J, L), and number of nuclei per myotube (Figure 3J, M) were all highly significantly (P<0.01) reduced after inducing differentiation for 2 days of $MF^{+/-}$ cells compared to WT cells, as was the myotube diameter at the maximum measured (Figure 3J, N). In addtion, the differentiation capacity and fusion ability of $MF^{+/-}$ cells were consistently significantly lower than WT cells during the ongoing differentiation process, as was the diameter of fused myotubes (Figure S3A-J). The reduced expression of myogenic differentiation markers further confirmed that the $MSTN^{Del273C}$ mutation with *FGF5* knockout consistently inhibits myogenic differentiation of skeletal muscle satellite cells (Figure S3K-N). Taken together, our results elucidated that the $MSTN^{Del273C}$ mutation with *FGF5* knockout promotes proliferation and inhibits myogenic differentiation of skeletal muscle satellite cells, and induces a smaller myotube diameter of myotubes, which may explain the muscle fiber hyperplasia phenotype and the decreased cross-sectional area of muscle fibers in $MF^{-/-}$ and $MF^{+/-}$ sheep.

3.4 The $MSTN^{Del273C}$ mutation with *FGF5* knockout contribute to muscle phenotype via MEK-ERK-FOSL1 axis

To elucidate the potential mechanism of the $MSTN^{Del273C}$ mutation with *FGF5* knockout result in smaller muscle fiber cross-sectional area and myotube diameter, the RNA-seq was performed in gluteus medius. GO and KEGG enrichment analysis indicating that differentially expressed genes (DEGs) were significantly closely related to cell proliferation, myogenic differentiation, and muscle development; and significantly enriched in MAPK signaling pathway (Figure 4A-B). Among DEGs, FOSL1 has aroused our interest. Compared to WT sheep, the FSOL1 mRNA level was significantly (P<0.05) lower in both gluteus medius and longissimus dorsi in $MF^{+/-}$ sheep (Figure 4C), but it was significantly (P<0.05) elevated in $MF^{+/-}$ cells at GM and DM2 (Figure 4D). More strikingly, FOSL1 mRNA level was strongly

(P<0.01) decreased after induced differentiation (Figure 5E), and its expression diminished continuously with the differentiation progress. These results suggested that FOSL1 may play a crucial role in the proliferation and myogenic differentiation of skeletal muscle satellite cells.

FOSL1 is a member of the AP-1 family, and another member of this family, c-Fos, inhibits myogenesis and MyoD1 expression by directly binding to the MyoD1 promoter region. Therefore, we speculated that FOSL1 might have similar functions to c-Fos. Subsequent protein-protein interaction (PPI) analysis further suggested that there was a potential interaction between FOSL1 and MyoD1 (Figure 5F). In addition, the c-Fos mRNA level was highly significantly (P<0.01) reduced in $MF^{+/-}$ myoblasts compared to WT cells, whereas the MyoD1 mRNA level was dramatically (P<0.01) increased (Figure 5G). We futher found that two bZIP recognition sites in the MyoD1 promoter region had the most significant binding potential to FOSL1 (Figure 5H-J). Subsequently, ChIP-qPCR confirmed that FOSL1 directly binds to these two bZIP recognition sites in the MyoD1 promoter region (Figure 5K-L). The dual luciferase report experiment confirmed that transcription factor FOSL1 can significantly (P<0.05) inhibit MyoD1 promoter activity (Figure 4M). These results indicated that FOSL1 plays an important role in the transcriptional regulation of MyoD1.

As mentioned above, FOSL1 may be involved in the proliferation and myogenic differentiation of skeletal muscle satellite cells. Here, the protein levels of FOSL1 and c-Fos were significantly (P<0.05) reduced in $MF^{+/-}$ cells at GM compared to WT cells (Figure 4N-O), and accompanied by a significant (P<0.05) increase in p-FOSL1 protein levels (Figure 4N-O), whereas FOSL1 protein levels were significantly (P<0.05) diminished and c-Fos protein levels were highly significantly (P<0.01) elevated in $MF^{+/-}$ cells after induced differentiation (Figure 4P-Q), these results further support the key role of FOSL1 on myogenesis. As demonstrated previously, enrichment analysis significantly enriched the MAPK signaling pathway. Compared to WT cells, ERK1/2 protein level was extremely significantly (P<0.01) decreased, and accompanied by a significant (P<0.05) increase in p-ERK1/2 protein levels (Figure 4N-O). After induced differentiation, although both MEK1/2 and ERK1/2 protein levels were dramatically (P<0.01) inhibited (Figure 4P-Q).

Considering the possible serum regulation of MSTN, we examined the effects of MSTN mutations on its receptors and downstream target genes, and observed that both MSTN receptors were significantly up-regulated (Figure S4A), whereas the expression of downstream Smand and Jun families was also inhibited to a varying degree (Figure S4B-C). Furthermore, serum from $MF^{+/-}$ sheep promoted the proliferation of skeletal muscle satellite cells (Figure S4D). *MSTN*^{Del273C} mutation with *FGF5* knockout promoted FOSL1 expression using WT sheep serum (Figure S4E), which was similar to the results of FBS culture and HS induction. The serum from $MF^{+/-}$ sheep strongly stimulated FOSL1 expression and the inhibition of MyoD1 (Figure S4F). These results suggest that serum regulation cannot be ignored after *MSTN*^{Del273C} mutation with *FGF5* knockout.

In summary, *MSTN*^{Del273C} mutation with *FGF5* knockout may regulate the expression and activity of FOSL1 via the MEK1/2-ERK1/2-FOSL1 axis to affect the proliferation and myogenic differentiation of skeletal muscle satellite cells, and further contribute to muscle phenotype.

3.5 FOSL1 expression and activity control the proliferation and myogenic differentiation of skeletal muscle satellite cells

To investigate the role of FOSL1 on the proliferation and myogenic differentiation of skeletal muscle satellite cells, we successfully constructed *FOSL1* gain-of-function model (Figure 5A). We found that overexpression of *FOSL1* significantly (P<0.05) promotes cell proliferation (Figure 5B-E), suppressed c-Fos mRNA level (Figure 5F) (P<0.05), and inhibited MyoD1 mRNA (P<0.01) and protein (P<0.05) levels (Figure 5F-H). These results are consistent with what we observed in $MF^{+/-}$ cells at GM, suggesting a potential inhibitory effect of FOSL1 protein on MyoD1. In addition, the protein levels of MyoD1, MyoG and MyHC were all significantly decreased (P<0.05), proving that the myogenic differentiation was inhibited after FOSL1 was overexpressed (Figure 5I-J). Subsequently, immunofluorescence staining further confirmed the significant (P<0.05) inhibitory effect on cell differentiation (Figure 5K-L). Also, the number of myotubes, the number of nuclei per myotube, and the myotube diameter were all significantly decreased (P<0.05) (Figure 5K, M-O). Complementarily, we also constructed *FOSL1*

loss-of-function model (Figure 6A). In contrast to what observed in FOSL1 overexpression, interference with FOSL1 inhibited skeletal muscle satellite cell proliferation (Figure 6B-E), elevated c-Fos and MyoD1 mRNA levels (Figure 6F) and significantly (P<0.05) increased MyoD1 protein level (Figure 6G-H). With myogenic differentiation markers were significantly up-regulated (Figure 6I-J), the myotube fusion index, the number of myotubes, the number of nuclei per myotube, and the myotube diameter were all significantly increased (Figure 6K-O). These results further demonstrated that elevated FOSL1 level inhibits myogenic differentiation and produces smaller myotubes.

To further ascertain this insight, the tert-butylhydroquinone (TBHQ), which can strongly activate ERK1/2 and increase p-ERK1/2 protein expression level, was used to activate ERK1/2 and act as an indirect activator of FOSL1. As expected, the addition of 20 μM TBHQ significantly (P<0.01) inhibited the myogenic differentiation of skeletal muscle satellite cells (Figure 7A-B). And, the number of myotubes was significantly increased (P<0.05) (Figure 7A, C), while the number of nuclei per myotube was significantly (P<0.05) decreased and produced a smaller myotube diameter (P<0.05) (Figure 7A, D-E). In addition, PD98509, which can inhibit ERK1/2 and dose-dependent reduce p-ERK1/2 protein expression level, was used for complementary experiments. We observed opposite results to TBHQ treatment, including increase in myotube fusion index, the number of nuclei per myotube, and the myotube diameter (Figure 7F-J). Taken together, our results shed light that the *MSTN*^{Del273C} mutation with *FGF5* knockout mediated the activation of FOSL1 via MEK-ERK-FOSL1 axis, further promotes skeletal muscle satellite cell proliferation, and inhibits myogenic differentiation by inhibiting the transcription of MyoD1, and resulting in smaller myotubes.

3.6 The *MSTN*^{Del273C} mutation with *FGF5* knockout inhibit calcium-dependent transcription signal pathway to regulate secondary fusion of myotubes

As mentioned previously, DEGs identified by RNA-seq were significantly enriched in biological processes such as muscle contraction and cardiac muscle contraction. In muscle contraction, calcium ions (Ca^{2+}) play a crucial role, triggering the process of muscle contraction and relaxation by binding to proteins in muscle

fibers. Here, the calcium-calmodulin dependent protein kinase II (CaMKII) α/δ protein level was significantly (P<0.05) reduced in $MF^{+/-}$ cells compared to WT cells (Figure 8A-B), and the intracellular Ca^{2+} concentration was also significantly (P<0.05) reduced (Figure 8C-D). The high-throughput Ca^{2+} channel RYR is responsible for rapid and massive release Ca^{2+} from the endoplasmic reticulum into cytoplasm. We observed a significant (P<0.05) decrease in RYR1 and/or RYR3 mRNA levels in $MF^{+/-}$ sheep skeletal muscle satellite cells and myotubes cells (Figure 8E-F). In addition, intracellular Ca^{2+} concentration correlated with myoblasts fusion, whereas the mRNA levels of MYMK and MYMX, which control myoblasts fusion, were significantly (P<0.01) reduced in $MF^{+/-}$ cells (Figure 8E-F). These results suggest that the decrease Ca^{2+} levels and inhibition of myoblasts fusion genes may be potential triggers for the decrease of myotube diameter and myofiber cross-sectional area in $MF^{+/-}$ sheep.

In a word, our results shed light that the *MSTN*^{Del273C} mutation with *FGF5* knockout mediated the activation of FOSL1 via MEK-ERK-FOSL1 axis (Figure 9). The activated FOSL1 promotes skeletal muscle satellite cell proliferation and inhibits myogenic differentiation by inhibiting the expression of MyoD1, and resulting in fusion to form smaller myotubes (Figure 9). In addition, activated ERK1/2 may inhibit the secondary fusion of myotubes by Ca^{2+}-dependent CaMKII activation pathway, leading to myoblasts fusion to form smaller myotubes (Figure 9).

4 Discussion

4.1 Optimized Cas9 mRNA and sgRNA delivery ratio improves the efficiency of dual-gene biallelic homozygous mutations

The strategy for producing gene knockout animals by CRISPR/Cas9 gene editing system is usually to introduce the Cas9 mRNA and the sgRNA of the target gene into their prokaryotic embryos by microinjection. However, this “one-step” method often results in a “mosaic” of gene-edited offspring (Wan *et al.*, 2015). Such chimeric mutants have now been reported in gene knockout mice (Wang *et al.*, 2013), rats (Bao *et al.*, 2015), monkeys (Niu *et al.*, 2014), pigs (Hai *et al.*, 2014), sheep (Hongbing HAN, 2014), goats (Wang *et al.*, 2015), rabbits (Lv *et al.*, 2016), and humans (Wang

and Yang, 2019) prepared by a “one-step” method using the CRISPR/Cas9 system. For studies involved in genetic phenotypes, chimeric gene knockout animals require further cross-breeding to obtain animals with a complete knockout of the target gene. Once required to generate multiple gene knockout animals, this time-consuming and laborious operation will become extremely difficult. Although many studies have been devoted to eliminating this widespread chimeric mutation (Sato *et al.*, 2015; Sung *et al.*, 2014; Kotani *et al.*, 2015; Chen *et al.*, 2015; Zhou *et al.*, 2014; Tu *et al.*, 2017; Wang *et al.*, 2015), however, these optimizations did not bring about a significant improvement in the production efficiency of biallelic knockout animals. Here, we increased the delivery ratio of Cas9 mRNA to sgRNA from 1:2 to 1:10, which improve the efficiency of the homozygous mutation of the biallelic gene. This unprecedented optimization method not only improved the overall gene knockout efficiency, but also the obtained gene-edited offspring were all dual-gene biallelic mutation. However, it is necessary to point out that although there are statistical differences, due to the limited number of sheep we actually produced and used for evaluation, the strategy to improve the efficiency of the homozygous mutation of biallelic gene by increasing the Cas9 and mRNA delivery ratio needs to be further comfirm in future studies.

4.2 Phenotypes produced by *MSTN* mutations are mutation site-dependent

As mentioned previously, although *MSTN* mutations have been found to produce a “double-muscle” phenotype in multiple species, the microscopic phenotypes are different, and this difference is closely related to the mutation site and species types. In mice, the number of skeletal muscle fibers with *MSTN* gene knockout significantly increased by 86% (McPherron *et al.*, 1997). A missense mutant *MSTN* only increased the number of mouse muscle fibers, while dominant negative *MSTN* resulted in increased muscle fiber cross-sectional area in mice, but not the number of muscle fibers (Nishi *et al.*, 2002; Zhu *et al.*, 2000). In addition, the use of *MSTN* neutralizing antibody on adult rats also resulted in an increased muscle fiber cross-sectional area (Haidet *et al.*, 2008). In cattle, natural MSTN mutant Belgian Blue cattle had an increased number of muscle fibers and reduced muscle fiber diameter (Wegner *et al.*, 2000). The muscle fiber cross-sectional area of longissimus dorsi and gluteus medius

in sheep was significantly increased after a 4bp deletion of the first exon of *MSTN* (Zhiliang *et al.*, 2004). In pigs, both the *MSTN* gene-edited Meishan and Hubei pigs showed a phenotype with increased muscle fiber density (Qian *et al.*, 2015; Xu *et al.*, 2013). Here, we prepared *MSTN*^{Del273C} mutation with *FGF5* knockout sheep with 3-base pairs of AGC in the third exon of *MSTN*, which caused the deletion of cysteine at amino acid position 273. Its macroscopic phenotype is similar to that of the MSTN-edited sheep with the first exon knocked out 4-base pairs. Both of them showed an abnormally developed “double-muscle” phenotype of hip muscle, but the *MSTN*^{Del273C} mutation with *FGF5* knockout sheep highlights a muscle fiber hyperplasia phenotype.

4.3 FOSL1 recognizes and binds to the MyoD1 promoter and inhibits its expression

As previously described, AP-1 family members play key roles in skeletal muscle cell proliferation, differentiation, and muscle development. In this study, AP-1 family member *FOSL1* was significantly reduced in MF$^{+/-}$ sheep, and its expression were drastically reduced during myogenic differentiation, which was consistent with the decrease of *FOSL1* expression during C2C12 differentiation (Tobin *et al.*, 2016). In addition, FOSL2, another AP-1 family member, can also inhibit myoblast differentiation (Alli *et al.*, 2013a), which may support the inhibitory effect of FOSL1 on myogenic differentiation. Therefore, *FOSL1* was recognized as a potential gatekeeper. It has been shown that *FOSL1* heterodimerizes with other transcription factors, such as the members of the bZIP family, and these dimers are either disabling the transcriptional activator complex or saving the interacting proteins from degradation in proteasomes (Sobolev *et al.*, 2022). Moreover, c-Fos, a member of the AP-1 family, has been shown to inhibit MyoD1 expression and myogenesis by directly binding to the MyoD1 promoter region (Li *et al.*, 1992). Therefore, we speculate that *FOSL1* may have similar functions to c-Fos. PPI analysis suggested a potential interaction between *FOSL1* and MyoD1. Subsequently, we confirmed that FOSL1 directly binds to two bZIP recognition sites in the MyoD1 promoter region, and inhibits MyoD1 promoter activity. Meanwhile, the overexpression and interference of FOSL1 further confirmed the inhibitory effect of FOSL1 on the

532 expression of MyoD1. In a word, these results fully support our hypothesis that
533 FOSL1 binds the MyoD1 promoter and inhibits its expression.

534 **4.4 The *MSTN*^{Del273C} mutation with *FGF5* knockout contribute to muscle**
535 **phenotype via MEK-ERK-FOSL1 axis**

536 The nonclassical pathway of MSTN involves PI3K/Akt/mTOR signaling
537 pathway and MAPK signaling pathway, which mainly includes ERKs, JNKs and p38
538 MAPK (Huang *et al.*, 2007; Gui *et al.*, 2012). All of those pathways are involved in
539 the signal transduction pathway of MSTN and mediate the transcription of MRFs
540 (Myogenin, Myf5, MyoD), MuRF-1 and Atrogin-1, to regulate myogenic
541 differentiation and skeletal muscle quality (Chen *et al.*, 2021b). *MSTN* induces muscle
542 fiber hypertrophy prior to satellite cell activation (Wang and McPherron, 2012) and
543 inhibits IGF-I-induced increase in myotube diameter through Akt signaling pathway
544 (Morissette *et al.*, 2009). In our study, the MSTN^{Del273C} mutation with FGF5 knockout
545 resulted in the inhibition of myogenic differentiation of skeletal muscle satellite cells,
546 and the number of myotubes and the myotube size were significantly reduced.

547 As previously described, the DEGs of gluteus medius RNA-seq were
548 significantly enriched in the MAPK signaling pathway. In fact, the MAPK signaling
549 pathway has been proven to be closely related to muscle development and myoblast
550 differentiation (Xie *et al.*, 2018; Segales *et al.*, 2016). For example, ERK1/2 promotes
551 myoblast proliferation in response to various growth factors (Campbell *et al.*, 1995),
552 inhibits signaling pathways that activate ERK1/2, or isolates ERK1/2 in the cytoplasm,
553 leading to cell cycle exit and cell differentiation (Jones *et al.*, 2001; Michailovici *et al.*,
554 2014). The RXR activity in myoblasts promotes myogenesis by regulating MyoD
555 expression and acting as a MyoG cofactor (Zhu *et al.*, 2009). Inhibition of MEK1/2
556 activates satellite cell differentiation in primary muscle fibers (Alli *et al.*, 2013b), and
557 also induces myogenic differentiation and excessive fusion (Eigler *et al.*, 2021). A
558 recent study on glioma showed that FOSL1 can be activated by the
559 Ras-MEK1/2-ERK1/2 axis in MAPK signaling pathway (Marques *et al.*, 2021).
560 Similarly, the activated MEK1/2-ERK1/2 axis in aged skeletal muscle also activates
561 FOSL1 and increases the abundance of FOSL1 and the trans-activation capacity of the
562 Fos-Jun heterodimer (Mathes *et al.*, 2021). In our study, the *MSTN*^{Del273C} mutation

with *FGF5* knockout regulates FOSL1 expression and activity through MEK1/2-ERK1/2-FOSL1 axis and activated FOSL1 further inhibits myogenic differentiation of skeletal muscle satellite cells, resulting in smaller myotube diameter. However, despite the high expression of p-FOSL1 in $MF^{+/-}$ myoblasts, it did not significantly inhibit the transcription of MyoD1, which may be related to a dramatic enhance in c-Fos, or there might be other parallel signaling pathways regulating MyoD1 after *MSTN*^{Del273C} mutation with *FGF5* knockout.

Furthermore, it has been demonstrated that the inhibition of MEK1/2 using MEK1/2-specific inhibitor PD184352 can significantly down-regulate FOSL1 expression (Mathes *et al.*, 2021). In our study, the indirect activation of FOSL1 by TBHQ can inhibit the myogenic differentiation of sheep skeletal muscle satellite cells, leading to reduced myoblast fusion capacity and smaller myotube diameter. In contrast, inhibition of the MEK1/2 pathway by PD98059 to suppress FOSL1 activity produced the opposite effect. Taken together, these results shed light on the potential mechanisms by which *MSTN*^{Del273C} mutation with *FGF5* knockout leads to increased myofiber numbers and decreased fiber cross-sectional area.

4.5 The *MSTN*^{Del273C} mutation with *FGF5* knockout may affect myoblasts fusion through ERK-mediated calcium dependent transcriptional signaling pathway

Ca^{2+} is recognized as a regulator of mammalian muscle fusion (Eigler *et al.*, 2021; Constantin *et al.*, 1996). The transient depletion of Ca^{2+} in the endoplasmic reticulum is associated with myoblast differentiation and fusion (Jones *et al.*, 2001). However, the signaling cascade leading to Ca^{2+}-mediated myoblast fusion remains unclear. Intracellular Ca^{2+} level is regulated by various Ca^{2+} voltage-gated channels, including but not limited to ryanodine receptors (RYR), which is the main Ca^{2+} release channel of the sarcoplasmic reticulum. CaMKII is a member of the calcium/calmodulin-dependent serine/threonine kinase family. CaMKII δ, CaMKII γ, and CaMKII β are the main isoforms expressed in skeletal muscle (Bayer *et al.*, 1996). Recent studies have shown that elevated intracellular Ca^{2+} level is crucial for myoblasts fusion and that Ca^{2+} signaling in newly formed myotubes occurs prior to the rapid growth stage of myotubes, indicating that Ca^{2+} released from the endoplasmic reticulum in early myotubes may promote secondary fusion of myoblasts

and myotube expansion (Eigler *et al.*, 2021). Further studies showed that Ca^{2+}-dependent activation of CaMKII is essential for myotubes expansion and may mediate myoblast-myotube fusion by regulating MYMK and Rac1, but it is not necessary for myoblast-myoblast fusion (Eigler *et al.*, 2021).

In our study, the *MSTN*^{Del273C} mutation with *FGF5* knockout resulted in a significant reduction of Ca^{2+} level and CaMKII α/δ protein level, and led to a decrease in myotube fusion capacity. Therefore, our results support that the increased p-ERK1/2 level promotes cell proliferation and inhibits myogenic differentiation in $MF^{+/-}$ sheep skeletal muscle satellite cells. Meanwhile, activated ERK1/2 further inhibited RYR activity by suppressing the phosphorylation of RXR, thereby reducing the release of endoplasmic reticulum Ca^{2+} and potentially inhibiting the secondary fusion of myotubes by Ca^{2+}-dependent CaMKII activation pathway, and further mediating myofiber hyperplasia.

5 Conclusion

In this study, we found that increasing the delivery ratio of Cas9 mRNA to sgRNA can improve the efficiency of the homozygous mutation of the biallelic gene. Based on this, we generated a *MSTN*^{Del273C} mutation with *FGF5* knockout sheep, a dual-gene biallelic homozygous mutant, which highlights a dominant “double-muscle” phenotype. Both F0 and F1 generation mutants highlight the excellent trait of high-yield meat and the more number of muscle fibers per unit area. Our results suggested the *MSTN*^{Del273C} mutation with *FGF5* knockout mediated the activation of FOSL1 via MEK-ERK-FOSL1 axis, further promotes skeletal muscle satellite cell proliferation, and inhibits myogenic differentiation by inhibiting the expression of MyoD1, and resulting in smaller myotubes. In addition, activated ERK1/2 may inhibit the secondary fusion of myotubes by Ca^{2+}-dependent CaMKII activation pathway, leading to myoblasts fusion to form smaller myotubes. This supports the myofiber hyperplasia that more number of muscle fibers and smaller cross sectional area, caused by the MSTN^{Del273C} mutation with FGF5 knockout.

Data availability statement

The raw sequence data reported in this paper have been deposited in the Genome Sequence Archive (Genomics, Proteomics & Bioinformatics 2021) in National Genomics Data Center (Nucleic Acids Res 2022), China National Center for Bioinformation / Beijing Institute of Genomics, Chinese Academy of Sciences (GSA: CRA008539) that are publicly accessible at https://ngdc.cncb.ac.cn/gsa.

Ethics statement

All experiments were performed in accordance with relevant guidelines and adhere to the ARRIVE guidelines (https://arriveguidelines.org/) for the reporting of animal experiments. All sheep are raised in accordance with the national feeding standard NT/T815-2004. All procedures performed were consistent with the National Research Council Guide for the Care and Use of Laboratory Animals. All experimental animal protocols were approved and performed in accordance with the requirements of the Animal Care and Use Committee at China Agricultural University (AW02012202-1-3).

Competing financial interests

The authors declare that there are no competing financial interests.

Author contributions

MMC performed the majority of experiments, data analysis, and drafted the manuscript. YZ performed a part of experiments and revised the manuscript. XLX, SJW and ZML helped with data analysis. XSZ, JLZ and XFG were responsible for the management of the feeding plant, slaughtering, and collecting samples. YMY helped to process some biological information data. SYQ, GY, SQW, HXL and AWW helped to collect and organize original data. GSL led the prokaryotic injection and embryo transfer. YL prepared the gene editing sheep. KY and HBH participated in project management. KY, FHL and ZXL conceived the project, revised manuscript and final approval of manuscript. All authors read and approved the final manuscript.

Acknowledgments

This work was supported by Major Agricultural Biological Breeding Project (2022ZD04014), National Key Research and Development Program-Key Projects (2021YFF1000704, 2021YFD1200900), Natural Science Foundation of China (32072722), and National Transgenic Creature Breeding Grand Project (2016zx08008-003).

Figure Legends

Figure 1 Efficient generation of sheep carrying biallelic mutations in dual gene via the CRISPR/Cas9 system

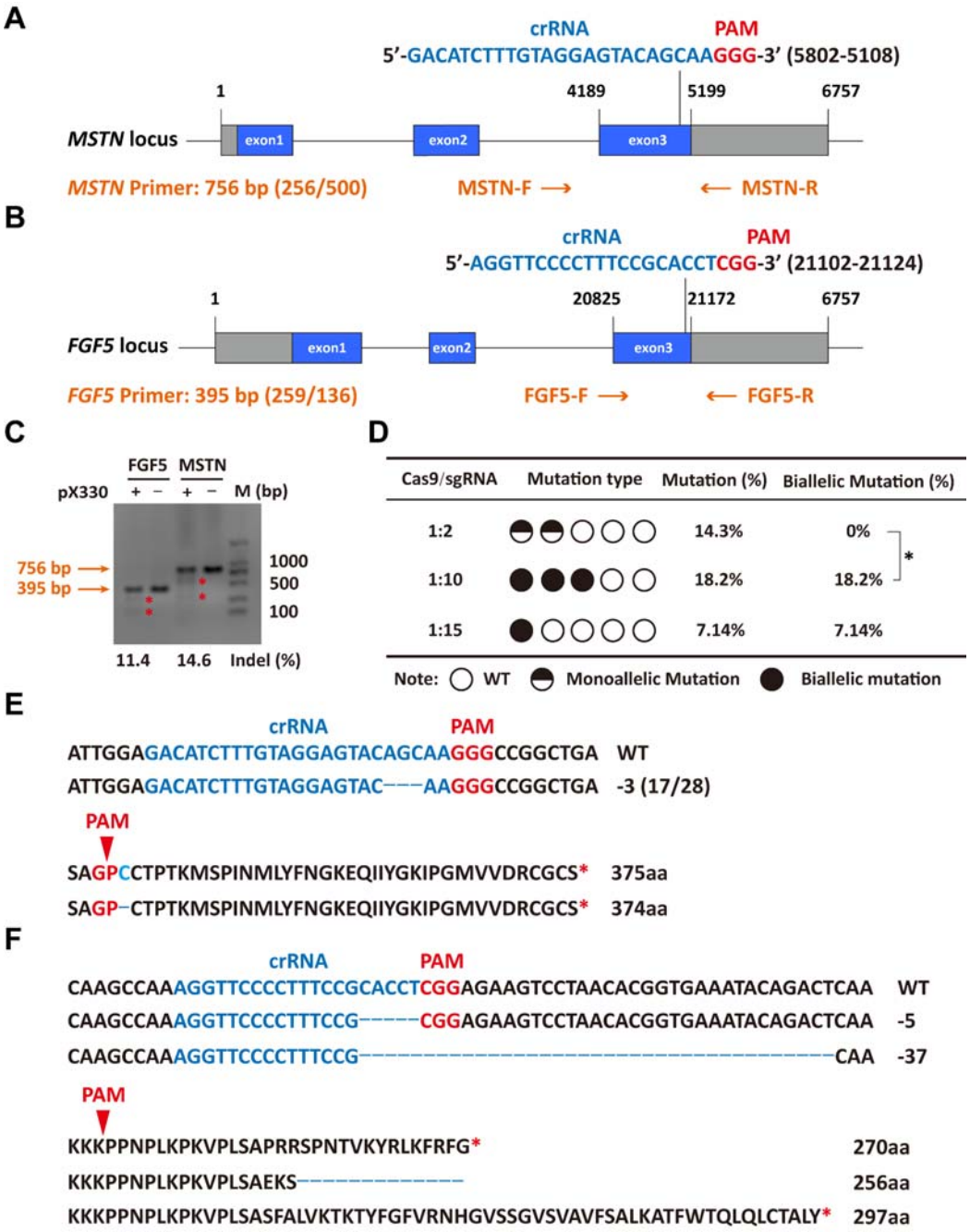

(A) Schematic of sgRNAs specific to exon 3 of the sheep MSTN locus. The crRNA sequences are highlighted in blue typeface and the PAM in red. (B) Schematic of sgRNAs specific to exon 3 of the sheep FGF5 locus. The crRNA sequences are

highlighted in blue typeface and the PAM in red. (C) T7EI assay for sgRNAs of MSTN and FGF5 in sheep fetal fibroblasts. The cleavage bands are marked with an red asterisk (*) and the indel frequencies were calculated using the expected fragments. (D) Summary of the generation of sheep carrying biallelic mutations in dual gene via zygote injection of Cas9 mRNA/sgRNAs. Biallelic mutation rate was statistically analyzed using chi square test. $*P < 0.05$. (E) Analysis of genome sequence and amino acid sequence of MSTN-modified sheep. The location of sgRNA and PAM are highlighted in blue and red, respectively. The deletions are indicated by a dashed line (-). (F) Analysis of genome sequence and amino acid sequence of FGF5-modified sheep. The location of sgRNA and PAM are highlighted in blue and red, respectively. The deletions are indicated by a dashed line (-).

Figure 2 The *MSTN*^{Del273C} mutation with *FGF5* knockout sheep highlights a dominant "double-muscle" phenotype and muscle fiber hyperplasia

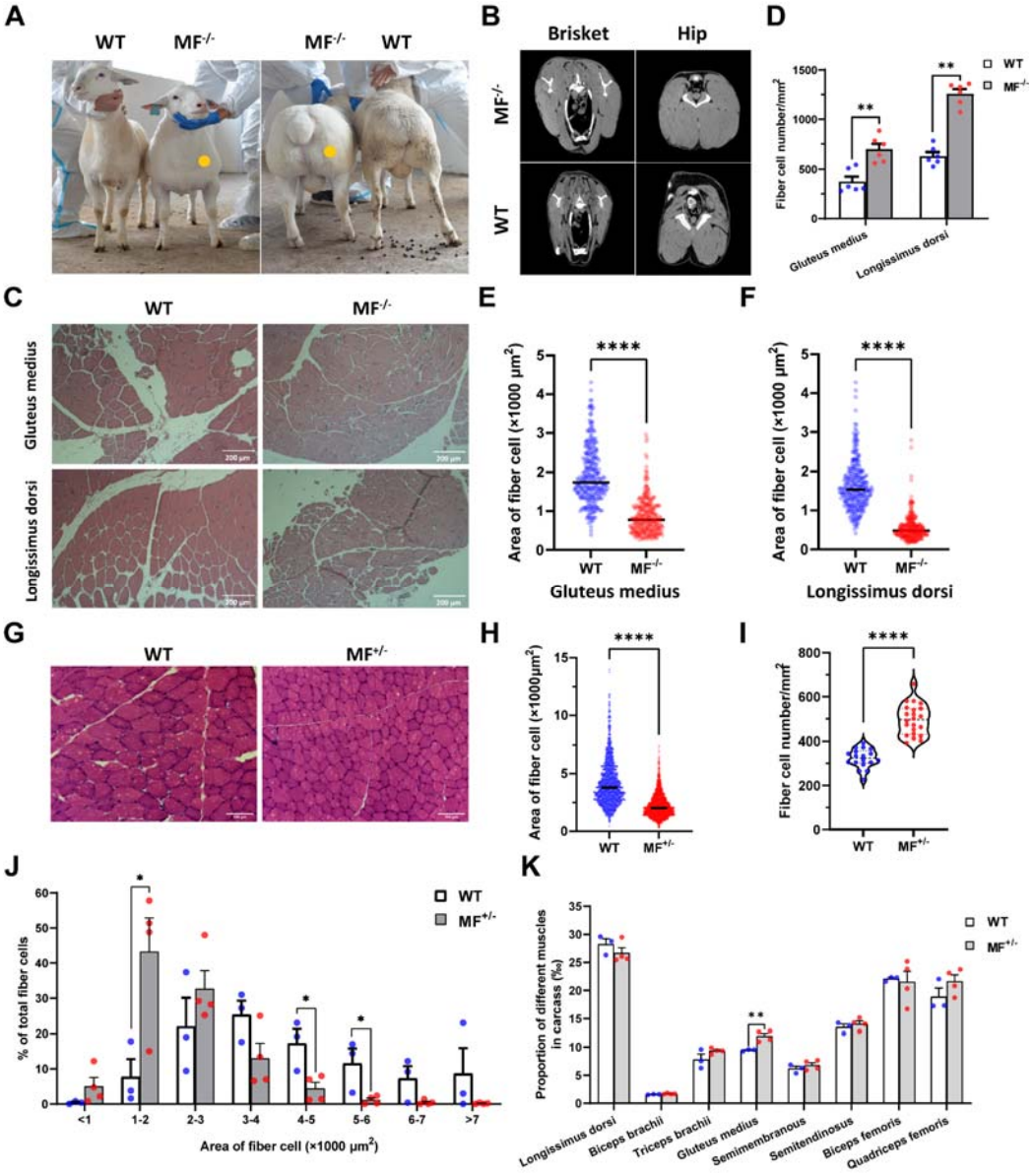

(A) The 6-month-old WT and MF$^{-/-}$ sheep. The genome-edited sheep displayed an obvious "double-muscle" phenotype compared with the WT. (B) The CT scanning image of the brisket and hip of WT and MF$^{-/-}$ sheep. (C) HE sections of gluteus medius and longissimus dorsi of WT and MF$^{-/-}$ sheep. Scale bar 200 μm. (D) Quantification of muscle fibre cell number of per unit area in WT (n=3) and MF$^{-/-}$ (n=1) sheep. All data points were shown. (E-F) Quantification of muscle fibre cell area of gluteus medius and longissimus dorsi in WT (n=3) and MF$^{-/-}$ (n=1) sheep. All

686 data points were shown. (G) HE sections of gluteus medius in WT and $MF^{+/-}$ sheep.
687 Scale bar 100 μm. (H) Quantification of muscle fibre cell area of gluteus medius in
688 WT (n=3) and $MF^{+/-}$ (n=4) sheep. (I) Quantification of muscle fibre cell number of
689 per unit area in WT (n=3) and $MF^{+/-}$ (n=4) sheep. (J) The percentage of
690 cross-sectional area of different size muscle fibers. (K) The proportion of different
691 muscles in carcass in WT (n=3) and $MF^{+/-}$ (n=4) sheep. Data: mean ± SEM. Unpaired
692 student's t-test were used for statistical analysis after the equal variance test,
693 otherwise the t-test with Welch's correction were performed. *P < 0.05, **P < 0.01,
694 ***P<0.001, and ****P<0.0001.
695

Figure 3 The *MSTN*^{Del273C} mutation with *FGF5* knockout promote proliferation and inhibit differentiation of skeletal muscle satellite cells

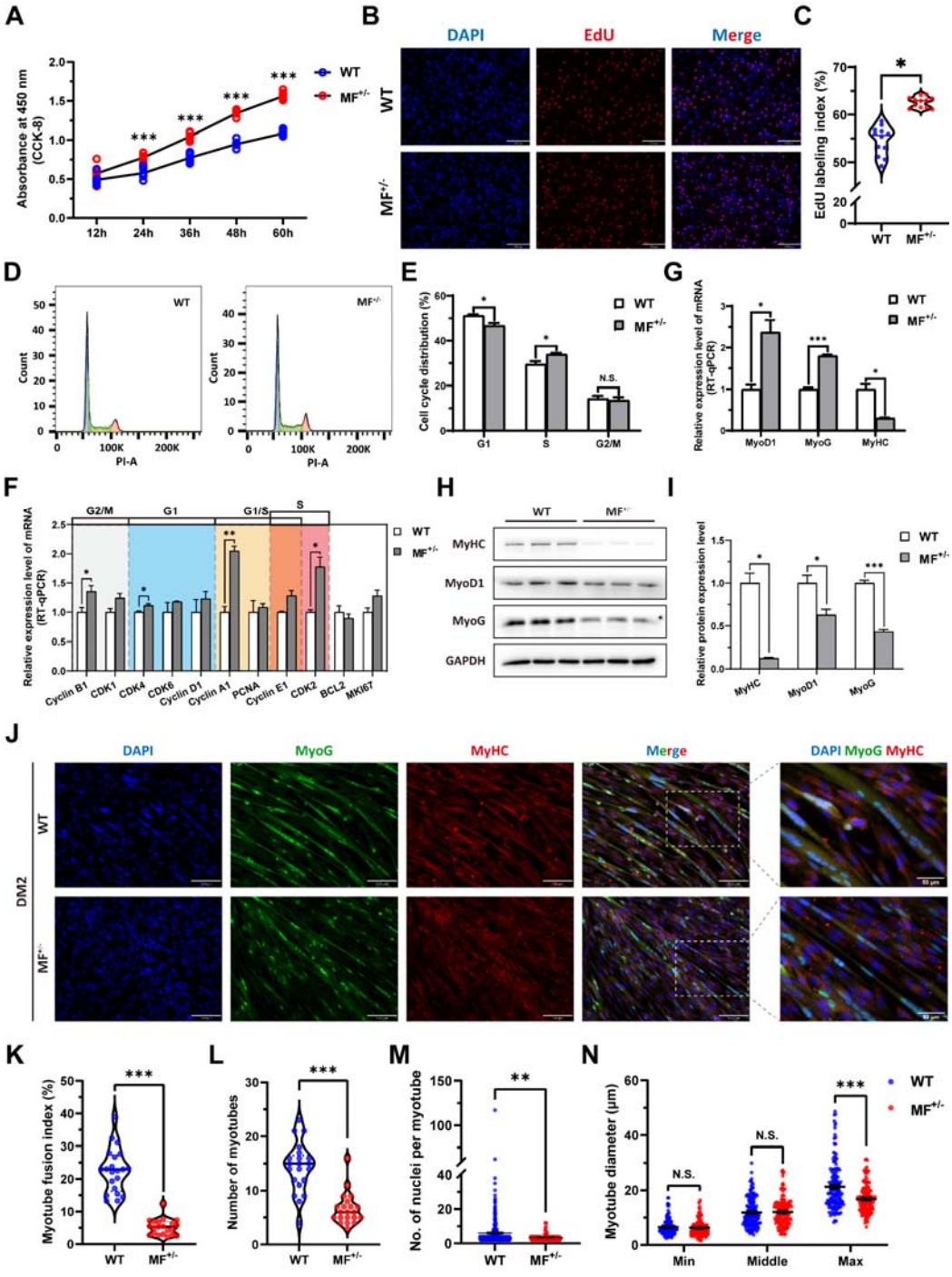

(A) The number of cells was detected by CCK-8 at 12h, 24h, 36h, 48h, and 60h in GM (n=7-8 per group). (B-C) EdU assay showed that the number of EdU positive cells and EdU labeling index were significantly increased in MF$^{+/-}$ cells (n=3). Scale

bar 130 μm. All data points were shown. (D-E) PI staining to detect cell cycle and showed a significant reduce in the proportion of G1 phase and a significant increase in the proportion of S phase in $MF^{+/-}$ cells (n=4). (F) The mRNA expression levels of cell cycle marker genes and cell proliferation marker genes (n=3). (G) The mRNA expression levels of myogenic differentiation marker genes MyoG, MyoD1, and MyHC (n=3). (H-I) The protein expression levels of myogenic differentiation marker genes MyoG, MyoD1, and MyHC (n=3). (J) The MyoG and MyHC immunofluorescence staining of myotubes in DM2. Scale bar 130 μm. (K) The myotube fusion index, which was represented by the number of cell nuclei in myotubes/total cell nuclei (n=3). All data points were shown. (L) The number of myotubes, which was the number of all myotubes in the field of view (n=3). All data points were shown. (M) The number of nuclei per myotube (n=3). All data points were shown. (N) The myotube diameter (n=3). To reflect the myotube diameter as accurately as possible, the vertical line at the thinnest position of the myotube is taken as the minimum measured (Min), the mid-perpendicular line of the long myotube axis is taken as the middle measured (Middle), and the vertical line at the widest position of the myotube is taken as the maximum measured (Max). All data points were shown. Data: mean ± SEM. Unpaired student's t-test and chi square test were used for statistical analysis. All student's t-test were performed after the equal variance test, otherwise the t-test with Welch's correction were used. $*P < 0.05$, $**P < 0.01$, and $***P<0.001$.

Figure 4 The *MSTN*^{Del273C} mutation with *FGF5* knockout contributes to muscle phenotype via MEK-ERK-FOSL1 axis

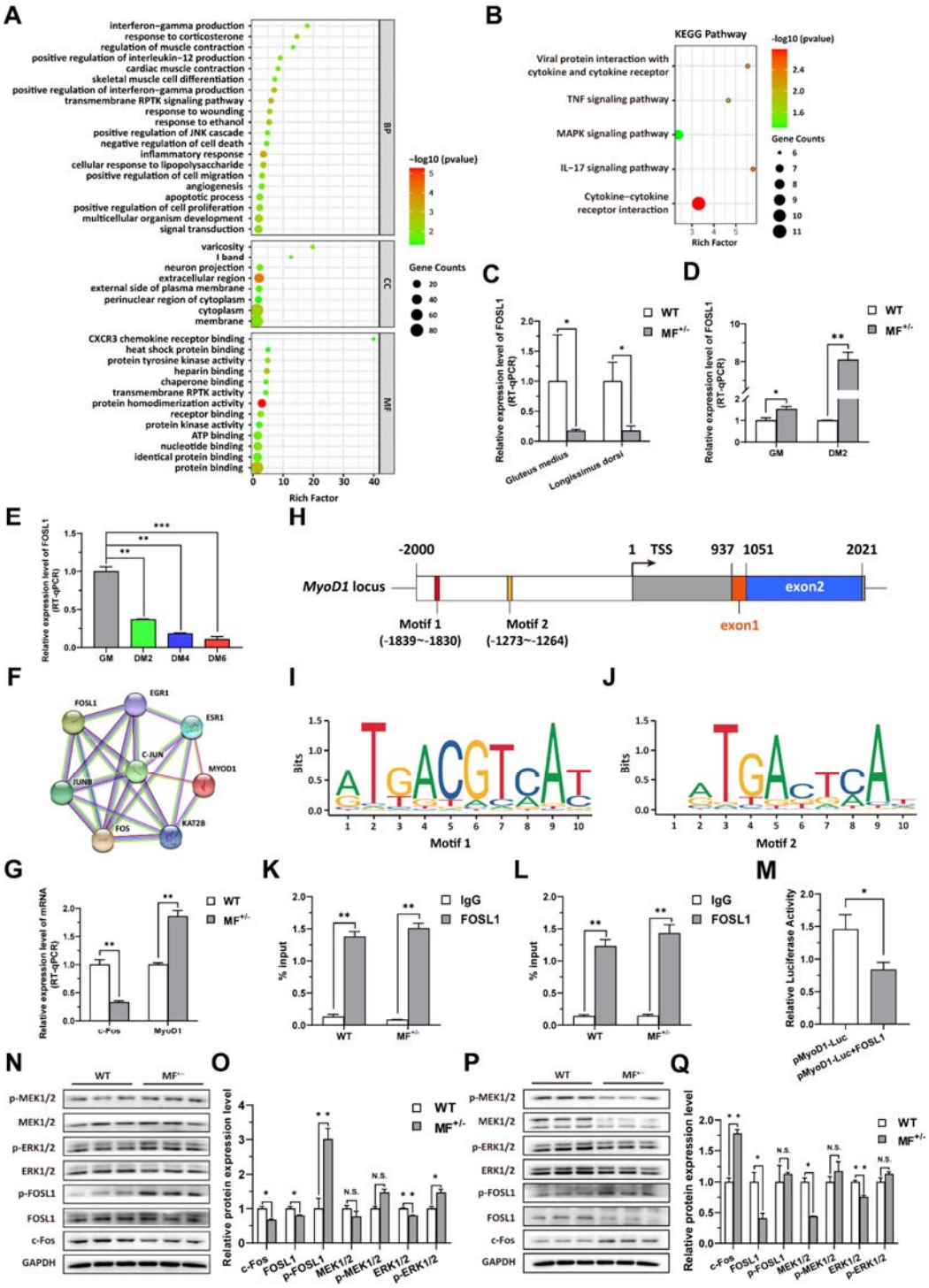

(A) Go enrichment analysis of DEGs. Among them, the top 20 entries with significant enrichment are listed in biological process (BP). CC, cellular component; MF,

molecular function. (B) KEGG enrichment analysis of DEGs. (C) The mRNA expression level of FOSL1 both at gluteus medius and longissimus dorsi in WT (n=3) and $MF^{+/-}$ (n=4) sheep. (D) The mRNA expression level of FOSL1 both at GM and DM2 in WT and $MF^{+/-}$ cells (n=3). (E) The expression level of FOSL1 mRNA during myogenic differentiation (n=3). (F) The protein-protein interaction (PPI) analysis of FOSL1, c-Fos and MyoD1. (G) The mRNA expression level of c-Fos and MyoD1 at GM in WT and $MF^{+/-}$ myoblasts (n=3). (H) Schematic diagram of MyoD1 gene body, promoter region and binding sites. (I-J) FOSL1 recognition motif in the MyoD1 promoter region. (K) FOSL1 ChIP-qPCR of motif 1 recognition region (n=3). (L) FOSL1 ChIP-qPCR of motif 2 recognition region (n=3). (M) Dual luciferase assay for the effect of FOSL1 on MyoD1 promoter activity (n=4). (N) Western blot of FOSL1, c-Fos, and key kinases of MAPK signaling pathways at GM. (O) Quantification of protein expression of FOSL1, c-Fos, and key kinases of MAPK signaling pathways at GM (n=3). (P) Western blot of FOSL1, c-Fos, and key kinases of MAPK signaling pathways at DM2. (Q) Quantification of protein expression of FOSL1, c-Fos, and key kinases of MAPK signaling pathways at DM2 (n=3). Data: mean ± SEM. Unpaired student's t-test was used for statistical analysis. All student's t-test were performed after the equal variance test, otherwise the t-test with Welch's correction were used. $*P < 0.05$, $**P < 0.01$, and $***P<0.001$.

Figure 5 The overexpression of *FOSL1* promotes proliferation and inhibits differentiation of skeletal muscle satellite cells

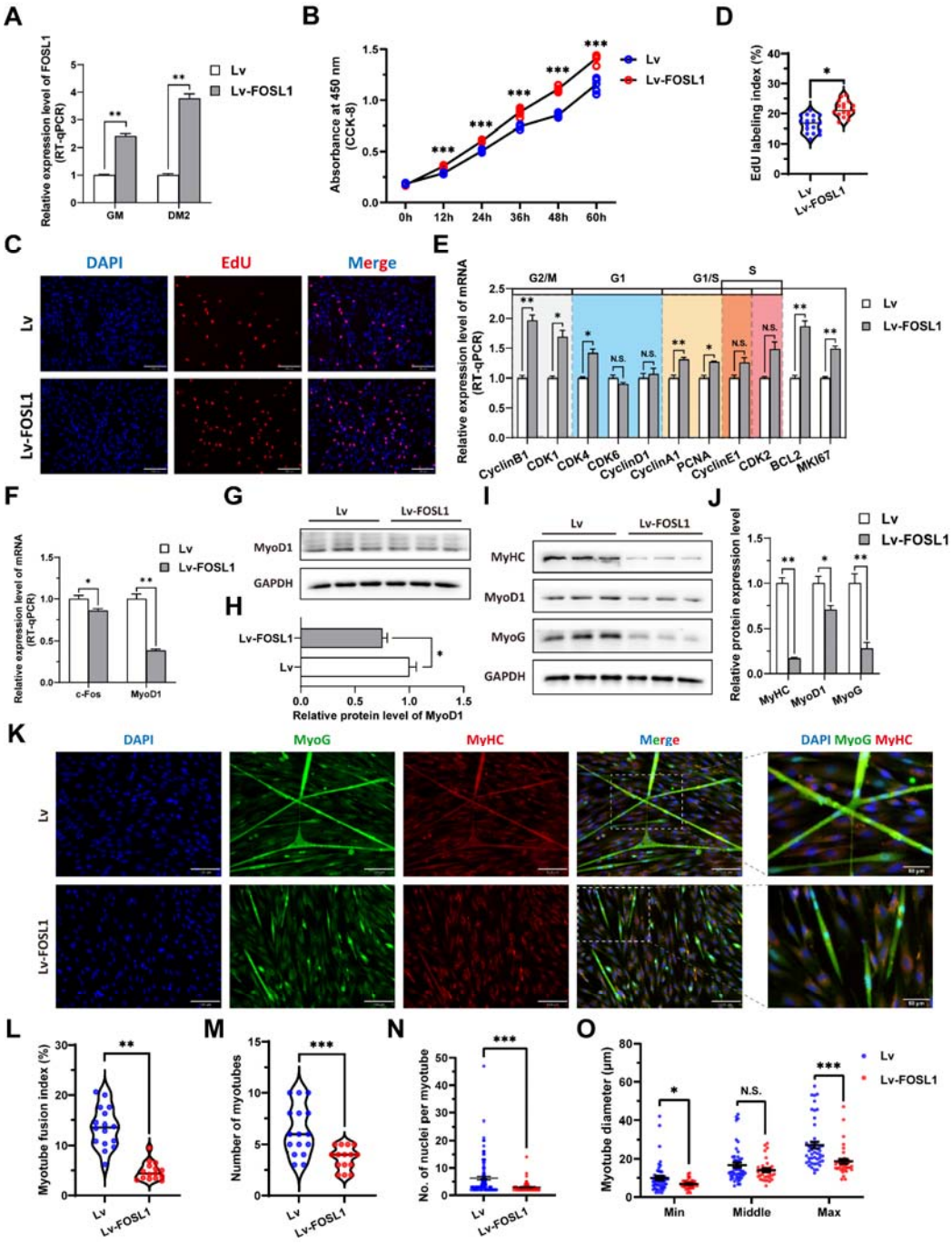

(A) The mRNA expression level of FOSL1 at GM and DM2 after lentivirus infection (n=3). (B) The number of cells detected by CCK-8 at 0h, 12h, 24h, 36h, 48h, and 60h after infection with lentivirus (n=4-6). (C-D) EdU assay showed that the number of EdU positive cells and EdU labeling index were significantly increased after infection

with lentivirus (n=3). Scale bar 130 μm. All data points were shown. (E) The mRNA expression levels of cell cycle marker genes and cell proliferation marker genes (n=3). (F) The mRNA expression levels of c-Fos and MyoD1 at GM after overexpression of FOSL1 (n=3). (G-H) The protein expression levels of MyoD1 at GM after overexpression of FOSL1 (n=3). (I-J) The protein expression levels of myogenic differentiation marker genes MyoD1, MyoG and MyHC at DM2 after overexpression of FOSL1 (n=3). (K) The MyoG and MyHC immunofluorescence staining of myotubes at DM2 after overexpression of FOSL1. Scale bar 130 μm. (L-O) The myotube fusion index, number of myotubes, number of nuclei per myotube and the myotube diameter at DM2 after overexpression of FOSL1 (n=3). All data points were shown. Data: mean ± SEM. Unpaired student's t-test and chi square test were used for statistical analysis. All student's t-test were performed after the equal variance test, otherwise the t-test with Welch's correction were used. *$P < 0.05$, **$P < 0.01$, and ***$P<0.001$.

Figure 6 The inhibition of *FOSL1* suppresses proliferation and promotes differentiation of skeletal muscle satellite cells

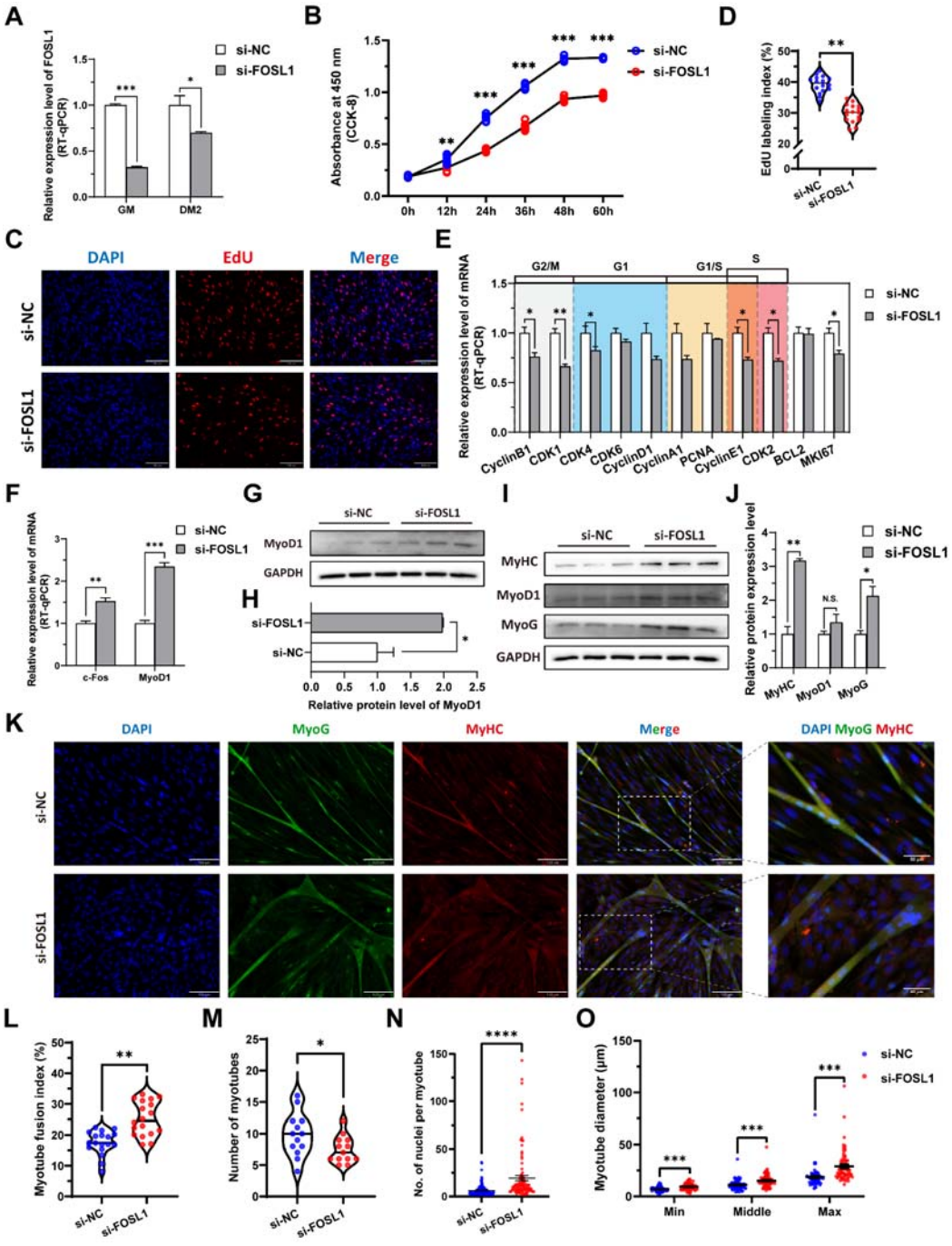

(A) The mRNA expression level of FOSL1 at GM and DM2 after inhibiting FOSL1 (n=3). (B) The number of cells detected by CCK-8 at 0h, 12h, 24h, 36h, 48h, and 60h after inhibiting FOSL1 (n=4-6). (C-D) EdU assay showed that the number of EdU positive cells and EdU labeling index were significantly decreased after inhibiting

778 FOSL1 (n=3). Scale bar 130 μm. All data points were shown. (E) The mRNA
779 expression levels of cell cycle marker genes and cell proliferation marker genes (n=3).
780 (F) The mRNA expression levels of c-Fos and MyoD1 at GM after inhibiting FOSL1
781 (n=3). (G-H) The protein expression levels of MyoD1 at GM after inhibiting FOSL1
782 (n=3). (I-J) The protein expression levels of myogenic differentiation marker genes
783 MyoD1, MyoG and MyHC at DM2 after inhibiting FOSL1 (n=3). (K) The MyoG and
784 MyHC immunofluorescence staining of myotubes at DM2 after inhibiting FOSL1.
785 Scale bar 130 μm. (L-O) The myotube fusion index, number of myotubes, number of
786 nuclei per myotube and the myotube diameter at DM2 after overexpression of FOSL1
787 (n=3). All data points were shown. Data: mean ± SEM. Unpaired student's t-test and
788 chi square test were used for statistical analysis. All student's t-test were performed
789 after the equal variance test, otherwise the t-test with Welch's correction were used.
790 *P < 0.05, **P < 0.01, ***P<0.001, and ****P<0.0001.
791
792

Figure 7 FOSL1 activity is a key regulator of myogenic differentiation and muscle myofiber hyperplasia

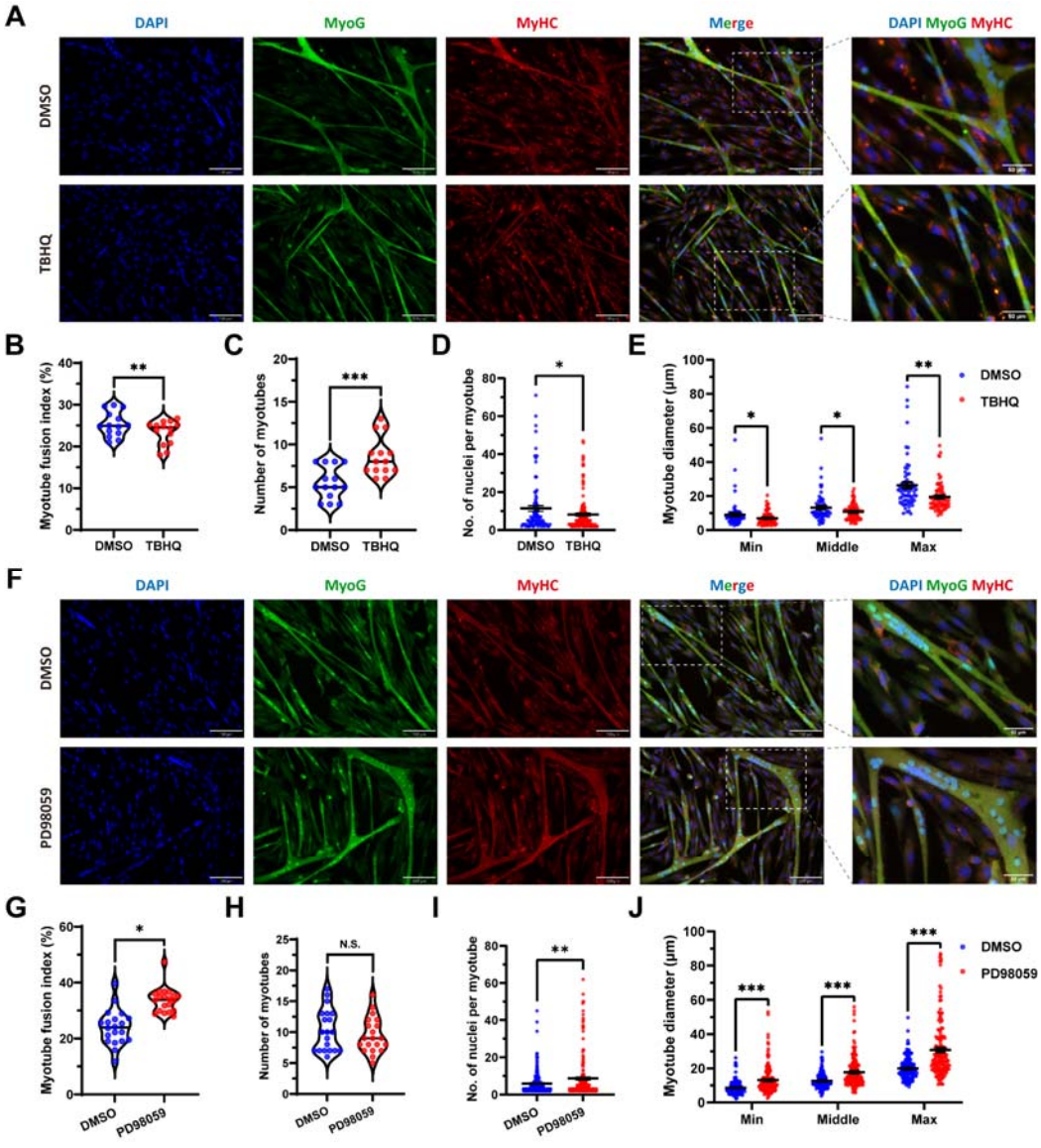

(A) Immunofluorescence staining of myogenic differentiation markers MyoG and MyHC in sheep skeletal muscle satellite cells at DM2 after addition of 20 μM TBHQ. Scale bar 130 μm or 50 μm. (B-E) The myotube fusion index, number of myotubes, number of nuclei per myotube and the myotube diameter at DM2 after addition of 20 μM TBHQ (n=3). All data points were shown. (F) Immunofluorescence staining of myogenic differentiation markers MyoG and MyHC in sheep skeletal muscle satellite cells at DM2 after addition of 1 μM PD98059. Scale bar 130 μm or 50 μm. (G-J) The myotube fusion index, number of myotubes, number of nuclei per myotube and the

804 myotube diameter at DM2 after addition of 1 μM PD98059 (n=3). All data points
805 were shown. Data: mean ± SEM. Unpaired student's t-test and chi square test were
806 used for statistical analysis. All student's t-test were performed after the equal
807 variance test, otherwise the t-test with Welch's correction were used. *$P < 0.05$, **$P <$
808 0.01, and ***$P<0.001$.
809

Figure 8 The *MSTN*^{Del273C} mutation with *FGF5* knockout inhibit calcium-dependent transcription signal pathway

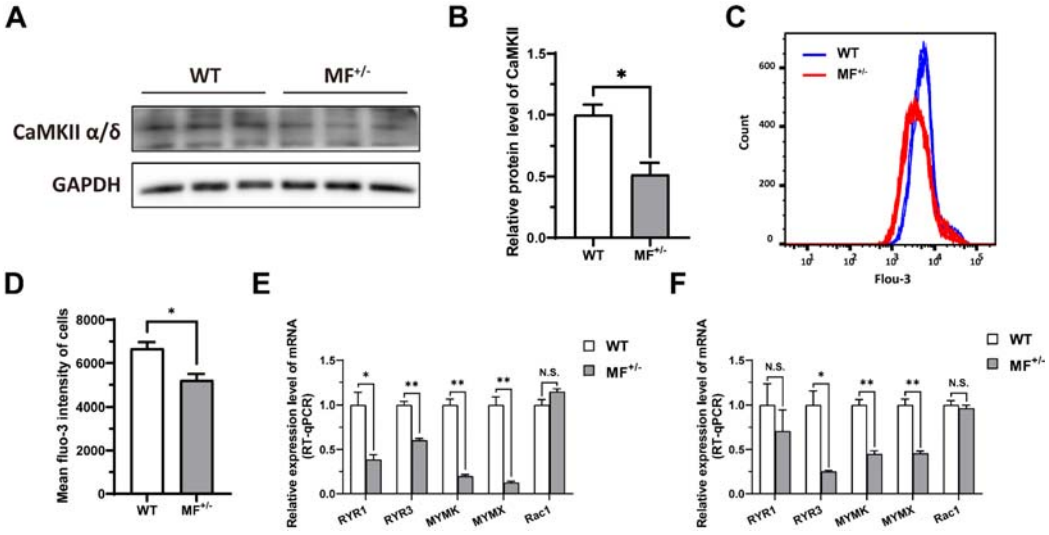

(A-B) The protein expression level of CaMKII α/δ between WT and MF$^{+/-}$ cells at GM (n=3). (C) Distribution of intracellular Ca^{2+} signals between WT and MF$^{+/-}$ cells at GM. (D) Average intracellular Ca^{2+} fluorescence intensity between WT and MF$^{+/-}$ cells at GM (n=4). (E) The mRNA expression levels of Ca^{2+} channels and myoblast fusion-related genes at GM (n=3). (F) The mRNA expression levels of Ca^{2+} channels and myoblast fusion-related genes at DM2 (n=3). Data: mean ± SEM. Unpaired student's t-test was used for statistical analysis. All student's t-test were performed after the equal variance test, otherwise the t-test with Welch's correction were used. **P* < 0.05, ***P* < 0.01.

Figure 9 Schematic illustration of the regulation of muscle phenotypes by *MSTN*^{Del273C} mutation with *FGF5* knockout

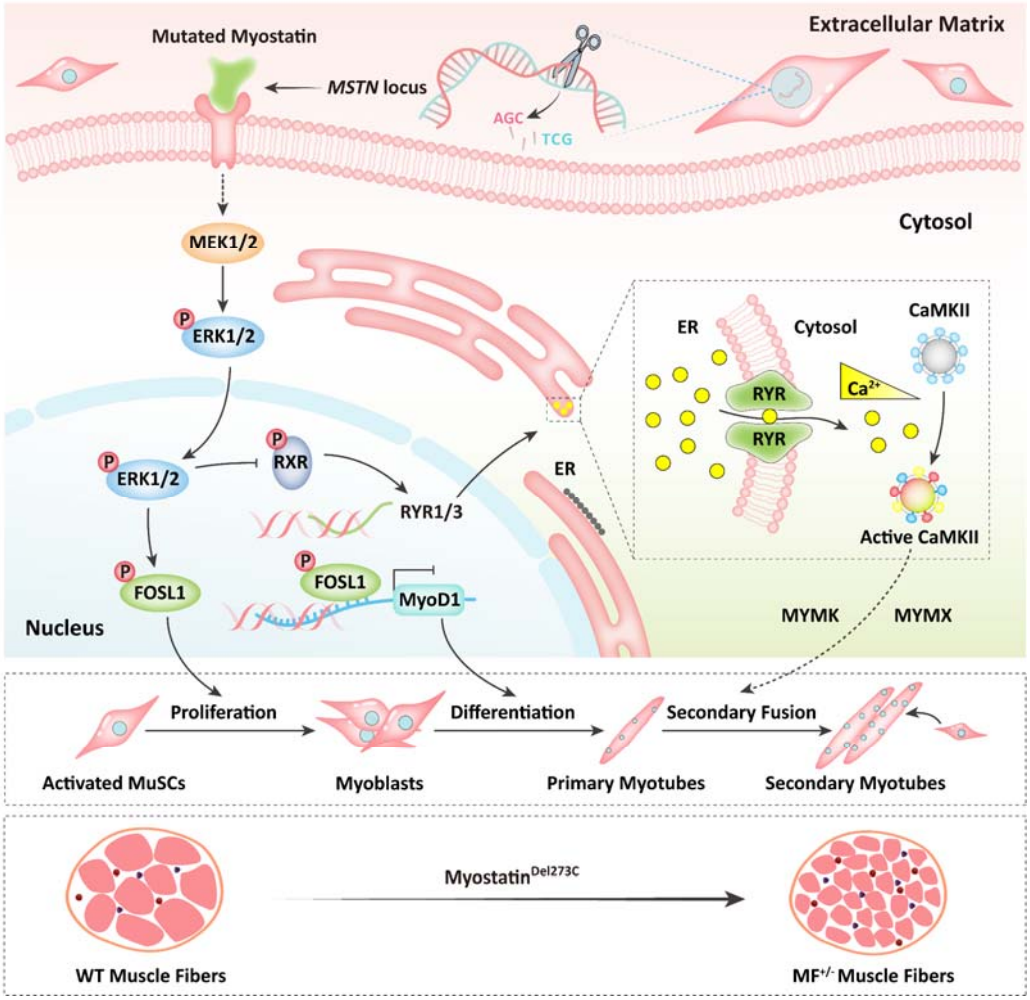

The *MSTN*^{Del273C} mutation with *FGF5* knockout mediated the activation of FOSL1 via MEK-ERK-FOSL1 axis. The activated FOSL1 promotes skeletal muscle satellite cell proliferation and inhibits myogenic differentiation by inhibiting the expression of MyoD1, and resulting in fusion to form smaller myotubes. In addition, activated ERK1/2 may inhibit the secondary fusion of myotubes by Ca^{2+}-dependent CaMKII activation pathway, leading to myoblasts fusion to form smaller myotubes.

834 **Figure S1 *FGF5* mutation does not affect muscle fiber size**

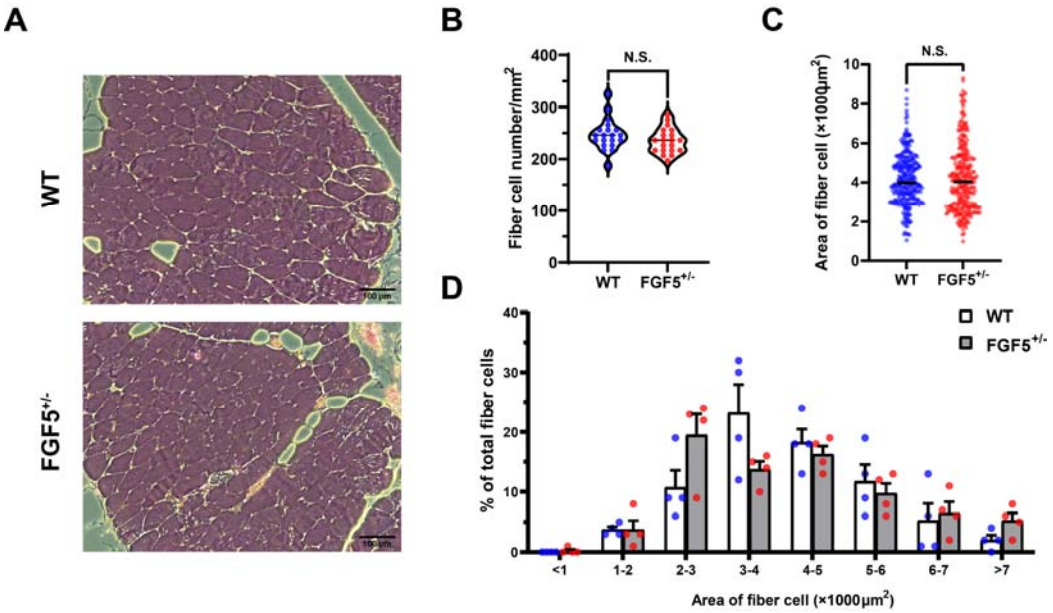

835

836 (A) HE sections of gluteus medius in WT and *FGF5*$^{+/-}$ sheep. Scale bar 100 μm. (B)
837 Quantification of muscle fibre cell area of gluteus medius in WT and *FGF5*$^{+/-}$ sheep.
838 (C) Quantification of muscle fibre cell number of per unit area in WT and *FGF5*$^{+/-}$
839 sheep. (D) The percentage of cross-sectional area of different size muscle fibers. Data:
840 mean ± SEM. Unpaired student's t-test was used for statistical analysis. All student's
841 t-test were performed after the equal variance test, otherwise the t-test with Welch's
842 correction were used.

843

844

845

Figure S2 The *MSTN*^{Del273C} mutation with *FGF5* knockout has no potential effect on MSTN expression and muscular dystrophy

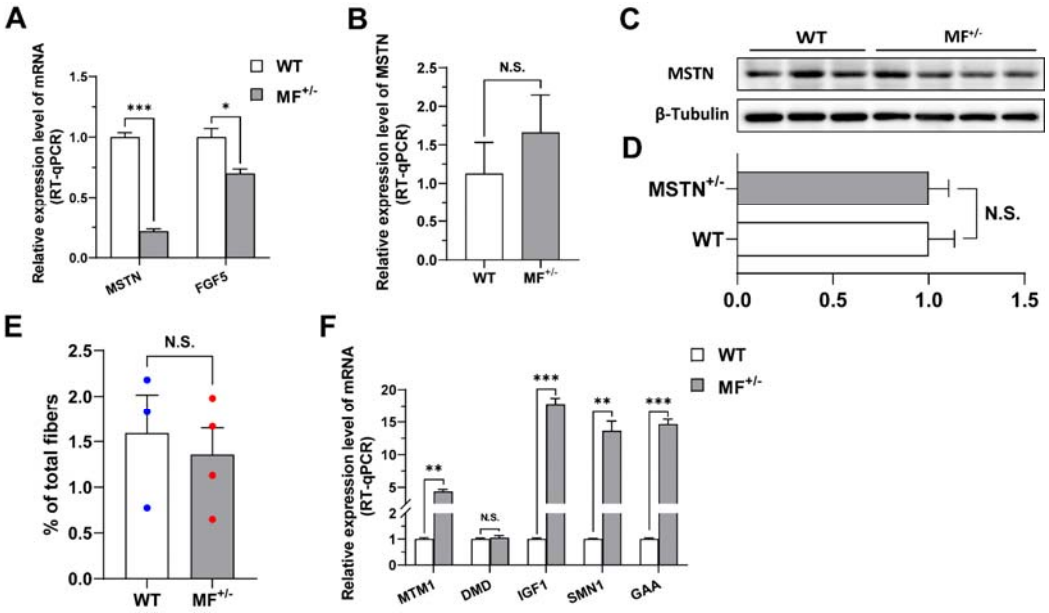

(A) The mRNA expression levels of *MSTN* and *FGF5* of gluteus medius in WT (n=4) and MF$^{+/-}$ (n=4) sheep at 3-month-old. (B) *MSTN* mRNA expression level of gluteus medius in WT (n=3) and MF$^{+/-}$ (n=4) sheep. (C-D) MSTN protein expression level of gluteus medius in WT (n=3) and MF$^{+/-}$ (n=4) sheep. (E) The proportion of centrally nucleated myofibres between WT (n=3) and MF$^{+/-}$ (n=4) sheep. (F) The mRNA expression of muscular dystrophy related genes between WT and MF$^{+/-}$ sheep (n=4). Data: mean ± SEM. Unpaired student's t-test was used for statistical analysis. All student's t-test were performed after the equal variance test, otherwise the t-test with Welch's correction were used. *P < 0.05, **P < 0.01, and ***P < 0.001.

Figure S3 The myogenic differentiation ability of $MF^{+/-}$ cells was continuously inhibited

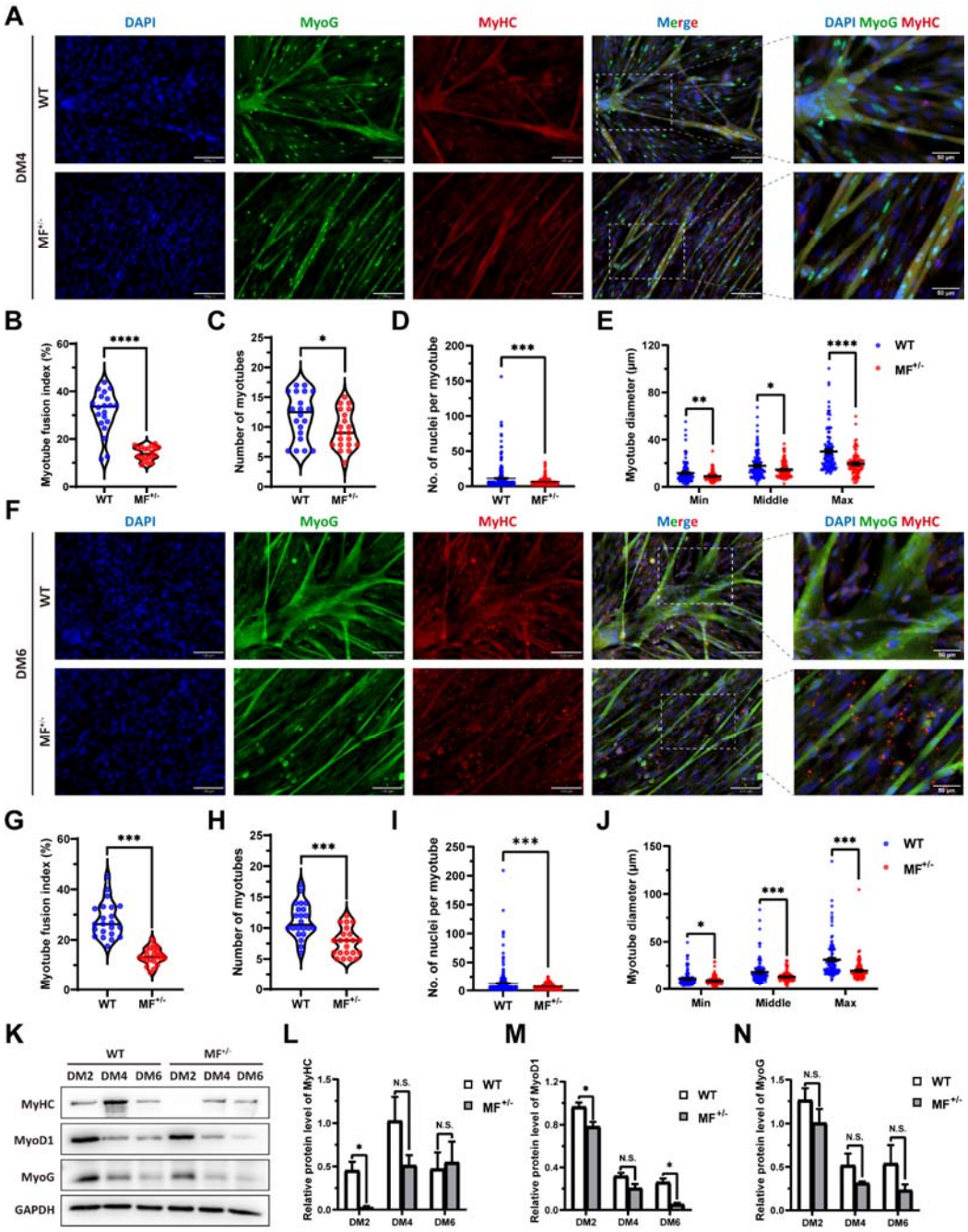

(A) The MyoG and MyHC immunofluorescence staining of myotubes at DM4. Scale bar 130 μm. (B-E) The myotube fusion index, number of myotubes, number of nuclei per myotube and the myotube diameter at DM4 (n=3). (F) The MyoG and MyHC immunofluorescence staining of myotubes at DM6. Scale bar 130 μm. (G-J) The myotube fusion index, number of myotubes, number of nuclei per myotube and the

867 myotube diameter at DM6 (n=3). (K-N) The protein expression levels of myogenic
868 differentiation markers during myogenic differentiation between WT and $MF^{+/-}$ cells
869 (n=2-3). Data: mean ± SEM. Unpaired student's t-test and chi square test were used
870 for statistical analysis. All student's t-test were performed after the equal variance test,
871 otherwise the t-test with Welch's correction were used. *P < 0.05, **P < 0.01,
872 ***P<0.001, and ****P<0.0001.

873 **Figure S4 The effects of MSTN signaling pathway and $MF^{+/-}$ serum on**
874 **proliferation and differentiation of skeletal muscle satellite cells**

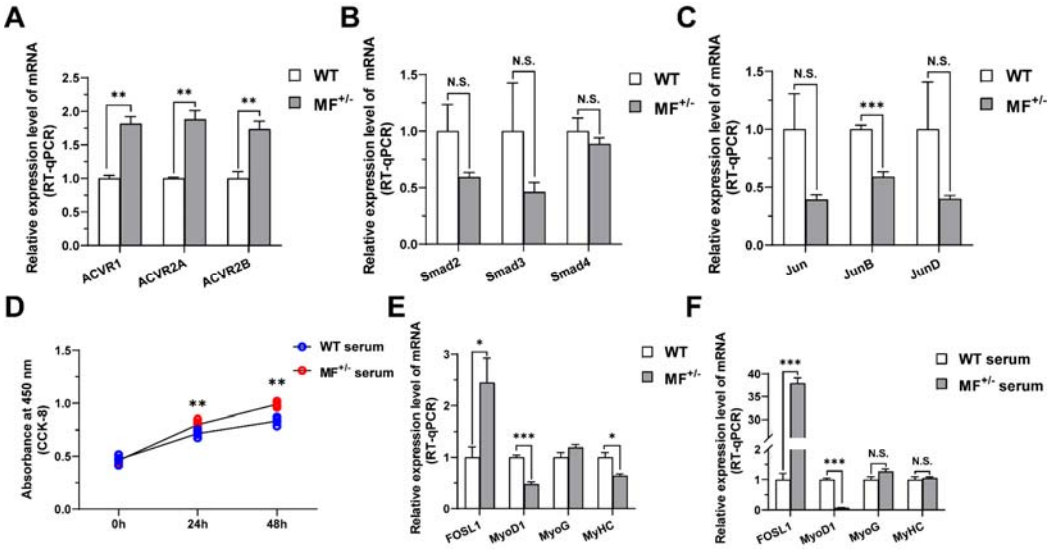

875

876 (A) The mRNA expression levels of type I and type II receptors of MSTN between
877 WT (n=3) and $MF^{+/-}$ (n=4) sheep gluteus medius. (B) The mRNA expression levels of
878 the Smad family downstream of MSTN between WT (n=3) and $MF^{+/-}$ (n=4) sheep
879 gluteus medius. (C) The mRNA expression levels of the Jun family downstream of
880 MSTN between WT (n=3) and $MF^{+/-}$ (n=4) sheep gluteus medius. (D) The number of
881 cells detected by CCK-8 at 0h, 24h, and 48h after culturing cells with serum from WT
882 sheep and $MF^{+/-}$ sheep (n=4-5). (E) The mRNA expression levels of FOSL1 and
883 myogenic differentiation markers between WT and $MF^{+/-}$ sheep skeletal muscle
884 satellite cells cultured and induced differentiation in sheep serum (n=4). (F) The
885 mRNA expression levels of FOSL1 and myogenic differentiation markers in skeletal
886 muscle satellite cells cultured and induced differentiation by serum from WT and
887 $MF^{+/-}$ sheep (n=4). Data: mean ± SEM. Unpaired student's t-test and chi square test
888 were used for statistical analysis. All student's t-test were performed after the equal
889 variance test, otherwise the t-test with Welch's correction were used. *P < 0.05, **P <
890 0.01, and ***P<0.001.

891

References

Alli, N. S., Yang, E. C., Miyake, T., Aziz, A., Collins-Hooper, H., Patel, K. & McDermott, J. C. (2013a). Signal-dependent fra-2 regulation in skeletal muscle reserve and satellite cells. *Cell Death Dis* 4: e692.

Alli, N. S., Yang, E. C., Miyake, T., Aziz, A., Collins-Hooper, H., Patel, K. & McDermott, J. C. (2013b). Signal-dependent fra-2 regulation in skeletal muscle reserve and satellite cells. *Cell Death Dis* 4(6): e692.

Baig, M. H., Ahmad, K., Moon, J. S., Park, S. Y., Ho Lim, J., Chun, H. J., Qadri, A. F., Hwang, Y. C., Jan, A. T., Ahmad, S. S., Ali, S., Shaikh, S., Lee, E. J. & Choi, I. (2022). Myostatin and its Regulation: A Comprehensive Review of Myostatin Inhibiting Strategies. *Front Physiol* 13: 876078.

Bao, D., Ma, Y., Zhang, X., Guan, F., Chen, W., Gao, K., Qin, C. & Zhang, L. (2015). Preliminary Characterization of a Leptin Receptor Knockout Rat Created by CRISPR/Cas9 System. *Sci Rep* 5: 15942.

Bayer, K. U., Lohler, J. & Harbers, K. (1996). An alternative, nonkinase product of the brain-specifically expressed Ca2+/calmodulin-dependent kinase II alpha isoform gene in skeletal muscle. *Mol Cell Biol* 16(1): 29-36.

Boman, I. A., Klemetsdal, G., Blichfeldt, T., Nafstad, O. & Vage, D. I. (2009). A frameshift mutation in the coding region of the myostatin gene (MSTN) affects carcass conformation and fatness in Norwegian White Sheep (Ovis aries). *Anim Genet* 40(4): 418-422.

Boman, I. A. & Vage, D. I. (2009). An insertion in the coding region of the myostatin (MSTN) gene affects carcass conformation and fatness in the Norwegian Spaelsau (Ovis aries). *BMC Res Notes* 2: 98.

Campbell, J. S., Wenderoth, M. P., Hauschka, S. D. & Krebs, E. G. (1995). Differential activation of mitogen-activated protein kinase in response to basic fibroblast growth factor in skeletal muscle cells. *Proc Natl Acad Sci U S A* 92(3): 870-874.

Chen, M., Zhang, L., Guo, Y., Liu, X., Song, Y., Li, X., Ding, X. & Guo, H. (2021a). A novel lncRNA promotes myogenesis of bovine skeletal muscle satellite cells via PFN1-RhoA/Rac1. *J Cell Mol Med*.

Chen, M. M., Zhao, Y. P., Zhao, Y., Deng, S. L. & Yu, K. (2021b). Regulation of Myostatin on the Growth and Development of Skeletal Muscle. *Front Cell Dev Biol* 9: 785712.

Chen, Y., Zheng, Y., Kang, Y., Yang, W., Niu, Y., Guo, X., Tu, Z., Si, C., Wang, H., Xing, R., Pu, X., Yang, S. H., Li, S., Ji, W. & Li, X. J. (2015). Functional disruption of the dystrophin gene in rhesus monkey using CRISPR/Cas9. *Hum Mol Genet* 24(13): 3764-3774.

Constantin, B., Cognard, C. & Raymond, G. (1996). Myoblast fusion requires cytosolic calcium elevation but not activation of voltage-dependent calcium channels. *Cell Calcium* 19(5): 365-374.

Dehnavi, E., Ahani Azari, M., Hasani, S., Nassiry, M. R., Mohajer, M., Khan Ahmadi, A., Shahmohamadi, L. & Yousefi, S. (2012). Polymorphism of Myostatin Gene in Intron 1 and 2 and Exon 3, and Their Associations with Yearling Weight, Using PCR-RFLP and PCR-SSCP Techniques in Zel Sheep. *Biotechnol Res Int* 2012: 472307.

Dierks, C., Momke, S., Philipp, U. & Distl, O. (2013). Allelic heterogeneity of FGF5 mutations causes the long-hair phenotype in dogs. *Anim Genet* 44(4): 425-431.

Dilger, A. C., Gabriel, S. R., Kutzler, L. W., McKeith, F. K. & Killefer, J. (2010). The myostatin null mutation and clenbuterol administration elicit additive effects in mice. *Animal* 4(3): 466-471.

Eigler, T., Zarfati, G., Amzallag, E., Sinha, S., Segev, N., Zabary, Y., Zaritsky, A., Shakked, A., Umansky, K. B., Schejter, E. D., Millay, D. P., Tzahor, E. & Avinoam, O. (2021). ERK1/2 inhibition promotes robust myotube growth via CaMKII activation resulting in myoblast-to-myotube fusion. *Dev Cell* 56(24): 3349-3363 e3346.

948 Fan, Z., Liu, Z., Xu, K., Wu, T., Ruan, J., Zheng, X., Bao, S., Mu, Y., Sonstegard, T. &
949 Li, K. (2022). Long-term, multidomain analyses to identify the breed and
950 allelic effects in MSTN-edited pigs to overcome lameness and sustainably
951 improve nutritional meat production. *Sci China Life Sci* 65(2): 362-375.
952 Grisolia, A. B., D'Angelo, G. T., Porto Neto, L. R., Siqueira, F. & Garcia, J. F. (2009).
953 Myostatin (GDF8) single nucleotide polymorphisms in Nellore cattle. *Genet*
954 *Mol Res* 8(3): 822-830.
955 Grobet, L., Martin, L. J., Poncelet, D., Pirottin, D., Brouwers, B., Riquet, J.,
956 Schoeberlein, A., Dunner, S., Menissier, F., Massabanda, J., Fries, R., Hanset,
957 R. & Georges, M. (1997). A deletion in the bovine myostatin gene causes the
958 double-muscled phenotype in cattle. *Nat Genet* 17(1): 71-74.
959 Gui, T., Sun, Y., Shimokado, A. & Muragaki, Y. (2012). The Roles of
960 Mitogen-Activated Protein Kinase Pathways in TGF-beta-Induced
961 Epithelial-Mesenchymal Transition. *J Signal Transduct* 2012: 289243.
962 Hai, T., Teng, F., Guo, R., Li, W. & Zhou, Q. (2014). One-step generation of knockout
963 pigs by zygote injection of CRISPR/Cas system. *Cell Res* 24(3): 372-375.
964 Haidet, A. M., Rizo, L., Handy, C., Umapathi, P., Eagle, A., Shilling, C., Boue, D.,
965 Martin, P. T., Sahenk, Z., Mendell, J. R. & Kaspar, B. K. (2008). Long-term
966 enhancement of skeletal muscle mass and strength by single gene
967 administration of myostatin inhibitors. *Proc Natl Acad Sci U S A* 105(11):
968 4318-4322.
969 Han, J., Forrest, R. H. & Hickford, J. G. (2013). Genetic variations in the myostatin
970 gene (MSTN) in New Zealand sheep breeds. *Mol Biol Rep* 40(11): 6379-6384.
971 Hanset, R. & Michaux, C. (1985). On the genetic determinism of muscular
972 hypertrophy in the Belgian White and Blue cattle breed. I. Experimental data.
973 *Genet Sel Evol (1983)* 17(3): 359-368.
974 Hebert, J. M., Rosenquist, T., Gotz, J. & Martin, G. R. (1994). FGF5 as a regulator of
975 the hair growth cycle: evidence from targeted and spontaneous mutations. *Cell*
976 78(6): 1017-1025.
977 Higgins, C. A., Petukhova, L., Harel, S., Ho, Y. Y., Drill, E., Shapiro, L., Wajid, M. &
978 Christiano, A. M. (2014). FGF5 is a crucial regulator of hair length in humans.
979 *Proc Natl Acad Sci U S A* 111(29): 10648-10653.
980 Hongbing HAN, Y. M., Tao WANG,Ling LIAN,Xiuzhi TIAN,Rui HU,Shoulong
981 DENG,Kongpan LI,Feng WANG,Ning LI,Guoshi LIU,Yaofeng
982 ZHAO,Zhengxing LIAN (2014). One-step generation of myostatin gene
983 knockout sheep via the CRISPR/Cas9 system. *Front. Agr. Sci. Eng.* 1(1): 2-5.
984 Huang, Z., Chen, D., Zhang, K., Yu, B., Chen, X. & Meng, J. (2007). Regulation of
985 myostatin signaling by c-Jun N-terminal kinase in C2C12 cells. *Cell Signal*
986 19(11): 2286-2295.
987 Jones, N. C., Fedorov, Y. V., Rosenthal, R. S. & Olwin, B. B. (2001). ERK1/2 is
988 required for myoblast proliferation but is dispensable for muscle gene
989 expression and cell fusion. *J Cell Physiol* 186(1): 104-115.
990 Kambadur, R., Sharma, M., Smith, T. P. & Bass, J. J. (1997). Mutations in myostatin
991 (GDF8) in double-muscled Belgian Blue and Piedmontese cattle. *Genome Res*
992 7(9): 910-916.
993 Kehler, J. S., David, V. A., Schaffer, A. A., Bajema, K., Eizirik, E., Ryugo, D. K.,
994 Hannah, S. S., O'Brien, S. J. & Menotti-Raymond, M. (2007). Four
995 independent mutations in the feline fibroblast growth factor 5 gene determine
996 the long-haired phenotype in domestic cats. *J Hered* 98(6): 555-566.
997 Kijas, J. W., McCulloch, R., Edwards, J. E., Oddy, V. H., Lee, S. H. & van der Werf, J.
998 (2007). Evidence for multiple alleles effecting muscling and fatness at the
999 ovine GDF8 locus. *BMC Genet* 8: 80.
1000 Kotani, H., Taimatsu, K., Ohga, R., Ota, S. & Kawahara, A. (2015). Efficient Multiple
1001 Genome Modifications Induced by the crRNAs, tracrRNA and Cas9 Protein
1002 Complex in Zebrafish. *PLoS One* 10(5): e0128319.
1003 Lee, S. J. (2021). Targeting the myostatin signaling pathway to treat muscle loss and
1004 metabolic dysfunction. *J Clin Invest* 131(9).

Legrand, R., Tiret, L. & Abitbol, M. (2014). Two recessive mutations in FGF5 are associated with the long-hair phenotype in donkeys. *Genet Sel Evol* 46: 65.

Li, L., Chambard, J. C., Karin, M. & Olson, E. N. (1992). Fos and Jun repress transcriptional activation by myogenin and MyoD: the amino terminus of Jun can mediate repression. *Genes Dev* 6(4): 676-689.

Li, Y., Lian, D., Deng, S., Zhang, X., Zhang, J., Li, W., Bai, H., Wang, Z., Wu, H., Fu, J., Han, H., Feng, J., Liu, G., Lian, L. & Lian, Z. (2016). Efficient production of pronuclear embryos in breeding and nonbreeding season for generating transgenic sheep overexpressing TLR4. *J Anim Sci Biotechnol* 7: 38.

Lv, Q., Yuan, L., Deng, J., Chen, M., Wang, Y., Zeng, J., Li, Z. & Lai, L. (2016). Efficient Generation of Myostatin Gene Mutated Rabbit by CRISPR/Cas9. *Sci Rep* 6: 25029.

Marchitelli, C., Savarese, M. C., Crisa, A., Nardone, A., Marsan, P. A. & Valentini, A. (2003). Double muscling in Marchigiana beef breed is caused by a stop codon in the third exon of myostatin gene. *Mamm Genome* 14(6): 392-395.

Marques, C., Unterkircher, T., Kroon, P., Oldrini, B., Izzo, A., Dramaretska, Y., Ferrarese, R., Kling, E., Schnell, O., Nelander, S., Wagner, E. F., Bakiri, L., Gargiulo, G., Carro, M. S. & Squatrito, M. (2021). NF1 regulates mesenchymal glioblastoma plasticity and aggressiveness through the AP-1 transcription factor FOSL1. *Elife* 10.

Mathes, S., Fahrner, A., Ghoshdastider, U., Rudiger, H. A., Leunig, M., Wolfrum, C. & Krutzfeldt, J. (2021). FGF-2-dependent signaling activated in aged human skeletal muscle promotes intramuscular adipogenesis. *Proc Natl Acad Sci U S A* 118(37).

McPherron, A. C., Lawler, A. M. & Lee, S. J. (1997). Regulation of skeletal muscle mass in mice by a new TGF-beta superfamily member. *Nature* 387(6628): 83-90.

Michailovici, I., Harrington, H. A., Azogui, H. H., Yahalom-Ronen, Y., Plotnikov, A., Ching, S., Stumpf, M. P., Klein, O. D., Seger, R. & Tzahor, E. (2014). Nuclear to cytoplasmic shuttling of ERK promotes differentiation of muscle stem/progenitor cells. *Development* 141(13): 2611-2620.

Morissette, M. R., Cook, S. A., Buranasombati, C., Rosenberg, M. A. & Rosenzweig, A. (2009). Myostatin inhibits IGF-I-induced myotube hypertrophy through Akt. *Am J Physiol Cell Physiol* 297(5): C1124-1132.

Nishi, M., Yasue, A., Nishimatu, S., Nohno, T., Yamaoka, T., Itakura, M., Moriyama, K., Ohuchi, H. & Noji, S. (2002). A missense mutant myostatin causes hyperplasia without hypertrophy in the mouse muscle. *Biochem Biophys Res Commun* 293(1): 247-251.

Niu, Y., Shen, B., Cui, Y., Chen, Y., Wang, J., Wang, L., Kang, Y., Zhao, X., Si, W., Li, W., Xiang, A. P., Zhou, J., Guo, X., Bi, Y., Si, C., Hu, B., Dong, G., Wang, H., Zhou, Z., Li, T., Tan, T., Pu, X., Wang, F., Ji, S., Zhou, Q., Huang, X., Ji, W. & Sha, J. (2014). Generation of gene-modified cynomolgus monkey via Cas9/RNA-mediated gene targeting in one-cell embryos. *Cell* 156(4): 836-843.

Pothuraju, M., Mishra, S. K., Kumar, S. N., Mohamed, N. F., Kataria, R. S., Yadav, D. K. & Arora, R. (2015). Polymorphism in the Coding Region Sequence of Gdf8 Gene in Indian Sheep. *Genetika* 51(11): 1297-1300.

Qian, L., Tang, M., Yang, J., Wang, Q., Cai, C., Jiang, S., Li, H., Jiang, K., Gao, P., Ma, D., Chen, Y., An, X., Li, K. & Cui, W. (2015). Targeted mutations in myostatin by zinc-finger nucleases result in double-muscled phenotype in Meishan pigs. *Sci Rep* 5: 14435.

Sato, M., Koriyama, M., Watanabe, S., Ohtsuka, M., Sakurai, T., Inada, E., Saitoh, I., Nakamura, S. & Miyoshi, K. (2015). Direct Injection of CRISPR/Cas9-Related mRNA into Cytoplasm of Parthenogenetically Activated Porcine Oocytes Causes Frequent Mosaicism for Indel Mutations. *Int J Mol Sci* 16(8): 17838-17856.

Segales, J., Perdiguero, E. & Munoz-Canoves, P. (2016). Regulation of Muscle Stem Cell Functions: A Focus on the p38 MAPK Signaling Pathway. *Front Cell Dev Biol* 4: 91.

Sjakste, T., Paramonova, N., Grislis, Z., Trapina, I. & Kairisa, D. (2011). Analysis of the single-nucleotide polymorphism in the 5'UTR and part of intron I of the sheep MSTN gene. *DNA Cell Biol* 30(7): 433-444.

Sobolev, V. V., Khashukoeva, A. Z., Evina, O. E., Geppe, N. A., Chebysheva, S. N., Korsunskaya, I. M., Tchepourina, E. & Mezentsev, A. (2022). Role of the Transcription Factor FOSL1 in Organ Development and Tumorigenesis. *Int J Mol Sci* 23(3).

Sundberg, J. P., Rourk, M. H., Boggess, D., Hogan, M. E., Sundberg, B. A. & Bertolino, A. P. (1997). Angora mouse mutation: altered hair cycle, follicular dystrophy, phenotypic maintenance of skin grafts, and changes in keratin expression. *Vet Pathol* 34(3): 171-179.

Sung, Y. H., Kim, J. M., Kim, H. T., Lee, J., Jeon, J., Jin, Y., Choi, J. H., Ban, Y. H., Ha, S. J., Kim, C. H., Lee, H. W. & Kim, J. S. (2014). Highly efficient gene knockout in mice and zebrafish with RNA-guided endonucleases. *Genome Res* 24(1): 125-131.

Tobin, S. W., Yang, D., Girgis, J., Farahzad, A., Blais, A. & McDermott, J. C. (2016). Regulation of Hspb7 by MEF2 and AP-1: implications for Hspb7 in muscle atrophy. *J Cell Sci* 129(21): 4076-4090.

Tu, Z., Yang, W., Yan, S., Yin, A., Gao, J., Liu, X., Zheng, Y., Zheng, J., Li, Z., Yang, S., Li, S., Guo, X. & Li, X. J. (2017). Promoting Cas9 degradation reduces mosaic mutations in non-human primate embryos. *Sci Rep* 7: 42081.

Wan, H., Feng, C., Teng, F., Yang, S., Hu, B., Niu, Y., Xiang, A. P., Fang, W., Ji, W., Li, W., Zhao, X. & Zhou, Q. (2015). One-step generation of p53 gene biallelic mutant Cynomolgus monkey via the CRISPR/Cas system. *Cell Res* 25(2): 258-261.

Wang, H. & Yang, H. (2019). Gene-edited babies: What went wrong and what could go wrong. *PLoS Biol* 17(4): e3000224.

Wang, H., Yang, H., Shivalila, C. S., Dawlaty, M. M., Cheng, A. W., Zhang, F. & Jaenisch, R. (2013). One-step generation of mice carrying mutations in multiple genes by CRISPR/Cas-mediated genome engineering. *Cell* 153(4): 910-918.

Wang, Q. & McPherron, A. C. (2012). Myostatin inhibition induces muscle fibre hypertrophy prior to satellite cell activation. *J Physiol* 590(9): 2151-2165.

Wang, X., Yu, H., Lei, A., Zhou, J., Zeng, W., Zhu, H., Dong, Z., Niu, Y., Shi, B., Cai, B., Liu, J., Huang, S., Yan, H., Zhao, X., Zhou, G., He, X., Chen, X., Yang, Y., Jiang, Y., Shi, L., Tian, X., Wang, Y., Ma, B., Huang, X., Qu, L. & Chen, Y. (2015). Generation of gene-modified goats targeting MSTN and FGF5 via zygote injection of CRISPR/Cas9 system. *Sci Rep* 5: 13878.

Wegner, J., Albrecht, E., Fiedler, I., Teuscher, F., Papstein, H. J. & Ender, K. (2000). Growth- and breed-related changes of muscle fiber characteristics in cattle. *J Anim Sci* 78(6): 1485-1496.

Wijaya, Y. T., Setiawan, T., Sari, I. N., Park, K., Lee, C. H., Cho, K. W., Lee, Y. K., Lim, J. Y., Yoon, J. K., Lee, S. H. & Kwon, H. Y. (2022). Ginsenoside Rd ameliorates muscle wasting by suppressing the signal transducer and activator of transcription 3 pathway. *J Cachexia Sarcopenia Muscle*.

Xie, S. J., Li, J. H., Chen, H. F., Tan, Y. Y., Liu, S. R., Zhang, Y., Xu, H., Yang, J. H., Liu, S., Zheng, L. L., Huang, M. B., Guo, Y. H., Zhang, Q., Zhou, H. & Qu, L. H. (2018). Inhibition of the JNK/MAPK signaling pathway by myogenesis-associated miRNAs is required for skeletal muscle development. *Cell Death Differ* 25(9): 1581-1597.

Xu, T. S., Gu, L. H., Zhang, X. H., Ye, B. G., Liu, X. L. & Hou, S. S. (2013). Characterization of myostatin gene (MSTN) of Pekin duck and the association of its polymorphism with breast muscle traits. *Genet Mol Res* 12(3): 3166-3177.

1118 Yoshizawa, Y., Wada, K., Shimoi, G., Kameyama, Y., Wakabayashi, Y., Fukuta, K. &
1119 Hashizume, R. (2015). A 1-bp deletion in Fgf5 causes male-dominant long
1120 hair in the Syrian hamster. *Mamm Genome* 26(11-12): 630-637.
1121 Zhang, R., Li, Y., Jia, K., Xu, X., Li, Y., Zhao, Y., Zhang, X., Zhang, J., Liu, G., Deng,
1122 S. & Lian, Z. (2020). Crosstalk between androgen and Wnt/beta-catenin leads
1123 to changes of wool density in FGF5-knockout sheep. *Cell Death Dis* 11(5):
1124 407.
1125 Zhiliang, G., Dahai, Z., Ning, L., Hui, L., Xuemei, D. & Changxin, W. (2004). The
1126 single nucleotide polymorphisms of the chicken myostatin gene are associated
1127 with skeletal muscle and adipose growth. *Sci China C Life Sci* 47(1): 25-30.
1128 Zhou, J., Wang, J., Shen, B., Chen, L., Su, Y., Yang, J., Zhang, W., Tian, X. & Huang,
1129 X. (2014). Dual sgRNAs facilitate CRISPR/Cas9-mediated mouse genome
1130 targeting. *FEBS J* 281(7): 1717-1725.
1131 Zhu, G. H., Huang, J., Bi, Y., Su, Y., Tang, Y., He, B. C., He, Y., Luo, J., Wang, Y.,
1132 Chen, L., Zuo, G. W., Jiang, W., Luo, Q., Shen, J., Liu, B., Zhang, W. L., Shi,
1133 Q., Zhang, B. Q., Kang, Q., Zhu, J., Tian, J., Luu, H. H., Haydon, R. C., Chen,
1134 Y. & He, T. C. (2009). Activation of RXR and RAR signaling promotes
1135 myogenic differentiation of myoblastic C2C12 cells. *Differentiation* 78(4):
1136 195-204.
1137 Zhu, X., Hadhazy, M., Wehling, M., Tidball, J. G. & McNally, E. M. (2000).
1138 Dominant negative myostatin produces hypertrophy without hyperplasia in
1139 muscle. *FEBS Lett* 474(1): 71-75.

1140